J|A|C|S ARTICLES

Published on Web 12/31/2009

# Probing Donor−Acceptor Interactions and *Co*-Conformational Changes in Redox Active Desymmetrized [2]Catenanes

Dennis Cao,[†] Matteo Amelia,[‡] Liana M. Klivansky,[†] Gayane Koshkakaryan,[†] Saeed I. Khan,[§] Monica Semeraro,[‡] Serena Silvi,[‡] Margherita Venturi,[‡] Alberto Credi,*[,‡] and Yi Liu*[,†]

*The Molecular Foundry, Lawrence Berkeley National Laboratory, One Cyclotron Road, Berkeley, California 94720, Department of Chemistry, University of California, Berkeley, California 94720, Dipartimento di Chimica "G. Ciamician", Università degli Studi di Bologna, via Selmi 2, 40126 Bologna, Italy, and Department of Chemistry and Biochemistry, University of California, Los Angeles, 405 Hilgard Avenue, Los Angeles, California 90095*

Received October 23, 2009; E-mail: alberto.credi@unibo.it; yliu@lbl.gov

***Abstract:*** We describe the synthesis and characterization of a series of desymmetrized donor−acceptor [2]catenanes where different donor and acceptor units are assembled within a confined catenated geometry. Remarkable translational selectivity is maintained in all cases, including two fully desymmetrized [2]catenanes where both donors and acceptors are different, as revealed by X-ray crystallography in the solid state, and by $^1$H NMR spectroscopy and electrochemistry in solution. In all desymmetrized [2]catenanes the *co*-conformation is dominated by the strongest donor and acceptor pairs, whose charge-transfer interactions also determine the visible absorption properties. Voltammetric and spectroelectrochemical experiments show that the catenanes can be reversibly switched among as many as seven states, characterized by distinct electronic and optical properties, by electrochemical stimulation in a relatively narrow and easily accessible potential window. Moreover in some of these compounds the oxidation of the electron donor units or the reduction of the electron acceptor ones causes the circumrotation of one molecular ring with respect to the other. These features make these compounds appealing for the development of molecular electronic devices and mechanical machines.

## Introduction

Since the first templated synthesis[1] of [2]catenanes, interlocked molecular systems[2] can now be obtained efficiently relying on supramolecular assistance to covalent synthesis. With the aid of preprogrammed interactions, such as hydrogen bonding,[3] $\pi$-stacking,[4] anion templating,[5] and metal−ligand coordination,[6] many assembly strategies have been developed for the synthesis of functional interlocked molecules. In particular, donor−acceptor interaction has become a favorable driving force in the synthesis of electro- and photoactive molecular machines on account of the rich electrochemical and photophysical properties of $\pi$-electron donors and acceptors. Mechanical motions generated from intercomponent movements render these nanoscale objects ideal candidates for molecular level switches. Indeed, molecular machines[7−9] of such kinds have been utilized to construct several devices,[10] including molecular memories,[11] smart surfaces,[12] nanovalves,[13] and molecular muscles.[14]

Desymmetrized [2]catenanes[15] serve as a role model of controllable molecular motors.[7,8d] Efficient rotary movements can be implemented only if precise control of translational isomerism is achieved. The synthesis of such compounds remains challenging as it requires the selection of pairs of complementary recognition units with distinctive binding strength and the proper assembly of such pairs into one molecular structure. Stoddart et al. reported a switchable [2]catenane[15f]

[†] Lawrence Berkeley National Laboratory and University of California, Berkeley.
[‡] Università di Bologna.
[§] University of California, Los Angeles.

(1) (a) Dietrich-Buchecker, C. O; Sauvage, J.-P. *Chem. Rev.* **1987**, *87*, 795–810. (b) *Templated Organic Synthesis*; Diederich, F., Stang, P. J., Ed.; Wiley-VCH: Weinheim, 1999. (c) *Molecular Catenanes, Rotaxanes and Knots: A Journey Through the World of Molecular Topology*; Sauvage, J.-P., Dietrich-Buchecker, C., Eds.; Wiley-VCH: Weinheim, Germany, 1999. (d) Breault, G. A.; Hunter, C. A.; Mayers, P. C. *Tetrahedron* **1999**, *55*, 5265–5293. (e) Hubin, T. J.; Busch, D. H. *Coord. Chem. Rev.* **2000**, *200*, 5–52. (f) Raehm, L.; Hamilton, D. G.; Sanders, J. K. M. *Synlett* **2002**, 1743–1761. (g) Kim, K. *Chem. Soc. Rev.* **2002**, *31*, 96–107. (h) Arico, F.; Badjic, J. D.; Cantrill, S. J.; Flood, A. H.; Leung, K. C.-F.; Liu, Y.; Stoddart, J. F. *Top. Curr. Chem.* **2005**, *249*, 203–259. (i) Dietrich-Buchecker, C.; Colasson, B. X.; Sauvage, J.-P. *Top. Curr. Chem.* **2005**, *249*, 261–283. (j) Kay, E. R.; Leigh, D. A. *Top. Curr. Chem.* **2005**, *262*, 133–177. (k) Loeb, S. J. *Chem. Commun.* **2005**, 1511–1518. (l) Flamigni, L.; Heitz, V.; Sauvage, J.-P. *Struct. Bonding (Berlin)* **2006**, *121*, 217–261. (m) Bogdan, A.; Rudzevich, Y.; Vysotsky, M. O.; Bohmer, V. *Chem. Commun.* **2006**, 2941–2952. (n) Nitschke, J. R. *Acc. Chem. Res.* **2007**, *40*, 103–112. (o) Loeb, S. J. *Chem. Soc. Rev.* **2007**, *36*, 226–235. (p) Lankshear, M. D.; Beer, P. D. *Acc. Chem. Res.* **2007**, *40*, 657–668. (q) Griffiths, K. E.; Stoddart, J. F. *Pure Appl. Chem.* **2008**, *80*, 485–506. (r) Dichtel, W. R.; Miljanic, O. S.; Zhang, W.; Spruell, J. M.; Patel, K.; Aprahamian, I.; Heath, J. R.; Stoddart, J. F. *Acc. Chem. Res.* **2008**, *41*, 1750–1761. (s) Haussmann, P. C.; Stoddart, J. F. *Chem. Rec.* **2009**, *9*, 136–154. (t) Faiz, J. A.; Heitz, V.; Sauvage, J.-P. *Chem. Soc. Rev.* **2009**, *38*, 422–442. (u) Chmielewski, M. J.; Davis, J. J.; Beer, P. D. *Org. Biomol. Chem.* **2009**, *7*, 415–424. (v) Mullen, K. M.; Beer, P. D. *Chem. Soc. Rev.* **2009**, *38*, 1701–1713.

 **10.1021/ja909041g** 

***Scheme 1.*** Synthetic Scheme for the Desymmetrized [2]Catenanes

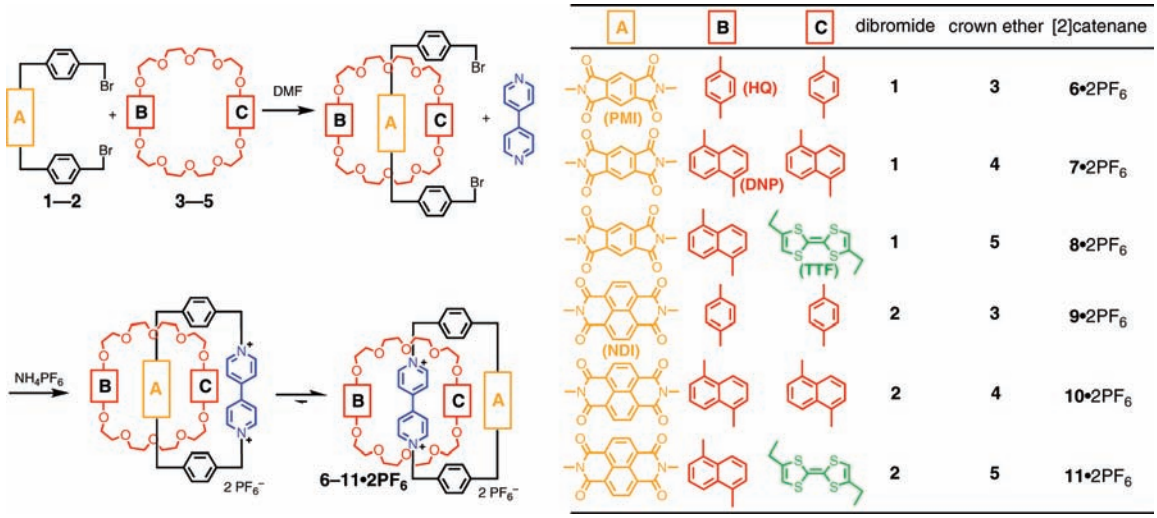


with a nearly "all-or-nothing" translational selectivity where two different $\pi$-donors, namely tetrathiafulvalene (TTF) and 1,5-dioxynaphthalene (DNP) moieties, were incorporated in a crown ether macrocyclic component that selectively holds the $\pi$-deficient tetracationic cyclophane around its TTF station as opposed to the DNP station. Another yet less explored way to implement control over the translational isomerism is to include two $\pi$-deficient units with considerably different $\pi$-accepting ability.[15c,g] Other than the well-known $\pi$-acceptor 4,4′-bipyridinium dication ($BPY^{2+}$), neutral naphthalene diimide (NDI) and pyromellitic diimide (PMI) units are readily available $\pi$-acceptors that have been incorporated in a variety of supramolecular systems.[16] Similar to $BPY^{2+}$ derivatives, they are able to form inclusion complexes with $\pi$-electron rich crown ethers. Their $\pi$-accepting ability, however, differs significantly. For example, the typical binding constants of a PMI and NDI derivative with 1,5-dinaphtho-38-crown-10 (DNP38C10) was only around 20 and 100 $M^{-1}$, respectively, while the binding constant between 1,1′-dibenzyl-4,4′-bipyridinium and DNP38C10 was around 20 000 $M^{-1}$.[15c,16j] The gradient in the $\pi$-accepting ability of these electron deficient units makes them attractive candidates as $\pi$-acceptors in desymmetrized [2]catenanes.

In a preliminary communication,[17] we demonstrated the feasibility of incorporating both $BPY^{2+}$ and PMI units in a $\pi$-deficient cyclophane component that interlocks with donor-containing crown ethers to give desymmetrized [2]catenanes. We intend to investigate these donor−acceptor based [2]catenanes (**6**−**11**•$2PF_6$, Scheme 1), with the scope of expanding [2]catenane synthesis by incorporating various donor−acceptor pairs. NDI units are successfully incorporated into a series of [2]catenanes as the secondary $\pi$-acceptors with $BPY^{2+}$ being the primary. In combination with a desymmetrized crown ether containing TTF and DNP as two different $\pi$-donors, [2]catenanes with four different donor and acceptor units are obtained. In all the [2]catenanes, the crown ether component is shown to encircle the $BPY^{2+}$ unit in both solution and the solid state, as revealed by $^1H$ NMR spectroscopic methods and X-ray single crystal structures. In the case of fully desymmetrized [2]catenanes, TTF is exclusively included in the dicationic cyclophane while the DNP unit lays alongside with the $BPY^{2+}$ unit. The set of [2]catenanes poise as an interesting collection of machine-like molecules with potential multistability that is endowed by mutual donor−acceptor interactions in a confined geometry. Extensive optical and electrochemical measurements have been conducted to gain more insight into the nature of the intercomponent interactions in these donor−acceptor systems. The interrogation of photophysical and electrochemical properties can also provide in-depth information of how to control *co*-conformational units by selectively modulating the electron density of the donors and acceptors.

## Experimental Section

Following a typical clipping protocol for [2]catenane synthesis, the desymmetrized [2]catenanes can be synthesized by a ring closure reaction to cyclize the $\pi$-electron deficient dicationic cyclophane around a templating $\pi$-electron rich crown ether. In consideration of the chemical sensitivity of $BPY^{2+}$, we decided to adapt a synthetic scheme such that this functionality is introduced at the

(2) (a) Schill, G. *Catenanes, Rotaxanes, and Knots*; Academic Press: New York, 1971. (b) Stoddart, J. F. *Chem. Soc. Rev.* **2009**, *38*, 1802–1820. (c) Coronado, E.; Gavina, P.; Tatay, S. *Chem. Soc. Rev.* **2009**, *38*, 1674–1689. (d) Leigh, D. A.; Lusby, P. J.; McBurney, R. T.; Morelli, A.; Slawin, A.; Thomson, A. R.; Walker, D. B. *J. Am. Chem. Soc.* **2009**, *131*, 3762–3771. (e) Stoddart, J. F. *Nat. Chem.* **2009**, *1*, 14–15.

(3) (a) Hunter, C. A. *J. Am. Chem. Soc.* **1992**, *114*, 5303–5311. (b) Johnston, A. G.; Leigh, D. A.; Pritchard, R. J.; Deegan, M. D. *Angew. Chem., Int. Ed. Engl.* **1995**, *107*, 1324–1327. (c) Vogtle, F.; Dunnwald, T.; Schmidt, T. *Acc. Chem. Res.* **1996**, *29*, 452–460. (d) Schalley, C. A.; Weilandt, T.; Brueggermann, J.; Voegtle, F. *Top. Curr. Chem.* **2005**, *248*, 141–200. (e) Janke, M.; Rudzevich, Y.; Molokanova, O.; Metzroth, T.; Mey, I.; Diezemann, G.; Marszalek, P. E.; Gauss, J.; Boehmer, V.; Janshoff, A. *Nat. Nanotech.* **2009**, *4*, 225–229.

(4) (a) Ashton, P. R.; Goodnow, T. T.; Kaifer, A. E.; Reddington, M. V.; Slawin, A. M. Z.; Spencer, N.; Stoddart, J. F.; Vicent, C.; Williams, D. J. *Angew. Chem., Int. Ed. Engl.* **1989**, *101*, 1404–1408. (b) Amabilino, D. B.; Stoddart, J. F. *Chem. Rev.* **1995**, *95*, 2725–2828. (c) Hamilton, D. G.; Sanders, J. K. M.; Davies, J. E.; Clegg, W.; Teat, S. J. *Chem. Commun.* **1997**, 897–898. (d) Hamilton, D. G.; Feeder, N.; Prodi, L.; Teat, S. J.; Clegg, W.; Sanders, J. K. M. *J. Am. Chem. Soc.* **1998**, *120*, 1096–1097. (e) Liu, Y.; Bonvallet, P. A.; Vignon, S. A.; Khan, S. I.; Stoddart, J. F. *Angew. Chem., Int. Ed.* **2005**, *44*, 3050–3055. (f) Miljanic, O. S.; Dichtel, W. R.; Khan, S. I.; Mortezaei, S.; Heath, J. R.; Stoddart, J. F. *J. Am. Chem. Soc.* **2007**, *129*, 8236–8246. (g) Nygaard, S.; Hansen, S. W.; Huffman, J. C.; Jensen, F.; Flood, A. H.; Jeppesen, J. O. *J. Am. Chem. Soc.* **2007**, *129*, 7354–7363. (h) Klivansky, L. M.; Koshkakaryan, G.; Cao, D.; Liu, Y. *Angew. Chem., Int. Ed.* **2009**, *48*, 4185–4189. (i) Li, S.; Liu, M.; Zheng, B.; Zhu, K.; Wang, F.; Li, N.; Zhao, X.; Huang, F. *Org. Lett.* **2009**, *11*, 3350–3353.

very end of the synthesis (Scheme 1). The reaction starts from an equilibrium involving an inclusion complex formed between a crown ether host and a reactive dibromide containing either PMI or NDI unit. After the addition of 4,4′-bipyridine into the reaction mixture, the bromides will be displaced upon nucleophilic attack of the pyridine to generate two $N^+-C$ bonds, commensurate with the formation of $BPY^{2+}$ unit. Only intramolecular $N^+-C$ bond formation is desirable for the formation of [2]catenanes while intermolecular reactions will lead to polymeric species. Thanks to the similar length (N−N distance around 7 Å) of $BPY^{2+}$, NDI, and PMI units, no significant geometrical restraints will impede the macrocyclization of [2]catenanes. On the other hand, the formation of $BPY^{2+}$ is facilitated by the donor−acceptor interactions reinforced in a fixed alternating geometry within a [2]catenane.

The synthesis is first carried out by reacting a PMI containing dibromide **1**, 4,4′-bipyridine, and a hydroquinone (HQ) containing crown ether, bis-*p*-phenylene[34]crown-10 (BPP34C10, **3**) in DMF (Scheme 1). After counterion exchange using an acetone/$NH_4PF_6$ mixture, the [2]catenane **6**•$2PF_6$ is isolated as a red solid in 30% yield. When the more electron rich crown ether 1,5-dinaphtho[38]crown-10 (DNP38C10, **4**) is used, the [2]catenane **7**•$2PF_6$ is isolated as a purple solid in 52% yield. NDI-containing [2]catenanes **9**•$2PF_6$ and **10**•$2PF_6$ are obtained in a similar fashion when dibromide **2** is employed.[18] The asymmetrical crown ether **5** containing TTF and DNP units as two different electron donors is prepared[15f] and subjected to clipping reactions to give fully desymmetrized [2]catenanes **8**•$2PF_6$ and **11**•$2PF_6$ as green solids.

**X-Ray Crystal Structural Analysis.** Although the $BPY^{2+}$ unit is known as a better electron acceptor than the PMI and NDI units when interacting with crown ethers, the *co*-conformation selectivity is to be tested when both $\pi$-acceptors are covalently linked in a [2]catenane setting. X-ray structural analysis provide clear evidence about the preference of $BPY^{2+}$ unit being included in the crown's cavity in the solid state in all [2]catenanes.[19] The crystal structure of **6**•$2PF_6$ and **7**•$2PF_6$ (Figure 1, a and b) indicates that the dicationic cyclophane is interlocked with the crown ethers such that (1) the HQ and DNP moieties are sandwiched between the nearly parallel-aligned $BPY^{2+}$ unit and PMI unit with (2) the $BPY^{2+}$ unit sandwiched between the parallel-aligned HQ and DNP moieties. The mean interplanar separations are 3.3 Å, in keeping with


(5) (a) Sambrook, M. R.; Beer, P. D.; Wisner, J. A.; Paul, R. L.; Cowley, A. R. *J. Am. Chem. Soc.* **2004**, *126*, 15364–15365. (b) Beer, P. D.; Sambrook, M. R.; Curiel, D. *Chem. Commun.* **2006**, 2105–2117. (c) Ng, K.-Y.; Cowley, A. R.; Beer, P. D. *Chem. Commun.* **2006**, 3676–3678. (d) Lankshear, M. D.; Beer, P. D. *Coord. Chem. Rev.* **2006**, *250*, 3142–3160. (e) Vickers, M. S.; Beer, P. D. *Chem. Soc. Rev.* **2007**, *36*, 211–225. (f) Ng, K.-Y.; Felix, V.; Santos, S. M.; Rees, N. H.; Beer, P. D. *Chem. Commun.* **2008**, 1281–1283. (g) Huang, B.; Santo, S. M.; Felix, V.; Beer, P. D. *Chem. Comm.* **2008**, *38*, 4610–4612.

(6) (a) Fujita, M.; Ibukuro, F.; Hagihar, H.; Ogura, K. *Nature* **1994**, *367*, 720–723. (b) Fujita, M.; Aoyagi, M.; Ibukuro, F.; Ogura, K.; Yamaguchi, K. *J. Am. Chem. Soc.* **1998**, *120*, 611–612. (c) Leigh, D. A.; Lusby, P. J.; Teat, S. J.; Wilson, A. J.; Wong, J. K. Y. *Angew. Chem., Int. Ed.* **2001**, *113*, 1586–1591. (d) Dietrich-Buchecker, C. O.; Colasson, B.; Fujita, M.; Hori, A.; Geum, N.; Sakamoto, S.; Yamaguchi, K.; Sauvage, J.-P. *J. Am. Chem. Soc.* **2003**, *125*, 5717–5725. (e) Fuller, A.-M.; Leigh, D. A.; Lusby, P. J.; Oswald, I. D. H.; Parsons, S.; Walker, D. B. *Angew. Chem., Int. Ed.* **2004**, *116*, 4004–4008. (f) Hogg, L.; Leigh, D. A.; Lusby, P. J.; Morelli, A.; Parsons, S.; Wong, J. K. Y. *Angew. Chem., Int. Ed.* **2004**, *116*, 1238–1241. (g) Hori, A.; Sawada, T.; Yamashita, K.; Fujita, M. *Angew. Chem., Int. Ed.* **2005**, *117*, 4974–4977. (h) Yamashita, K.; Kawano, M.; Fujita, M. *J. Am. Chem. Soc.* **2007**, *129*, 1850–1851. (i) Wu, J.; Fang, F.; Lu, W.-Y.; Hou, J.-L.; Li, C.; Wu, Z.-Q.; Jiang, X.-K.; Li, Z.-T.; Yu, Y.-H. *J. Org. Chem.* **2007**, *72*, 2897–2905. (j) Blight, B. A.; Wisner, J. A.; Jennings, M. C. *Angew. Chem., Int. Ed.* **2007**, *119*, 2893–2896. (k) Crowley, J. D.; Goldup, S. M.; Lee, A.-L.; Leigh, D. A.; McBurney, R. T. *Chem. Soc. Rev.* **2009**, *38*, 1530–1541.

(7) Balzani, V.; Credi, A.; Venturi, M. *Molecular Devices and Machines - Concepts and Perspectives for the Nanoworld*; Wiley-VCH: Weinheim, 2008.

(8) (a) Balzani, V.; Credi, A.; Raymo, F. M.; Stoddart, J. F. *Angew. Chem., Int. Ed.* **2000**, *112*, 3484–3530. (b) Browne, W. R.; Feringa, B. L. *Nat. Nanotechnol.* **2006**, *1*, 25–35. (c) Champin, B.; Mobian, P.; Sauvage, J.-P. *Chem. Soc. Rev.* **2007**, *36*, 358–366. (d) Kay, E. R.; Leigh, D. A.; Zerbetto, F. *Angew. Chem., Int. Ed.* **2007**, *46*, 72–191.

(9) (a) Tseng, H.-R.; Vignon, S. A.; Stoddart, J. F. *Angew. Chem., Int. Ed.* **2003**, *43*, 1491–1495. (b) Badjic, J. D.; Balzani, V.; Credi, A.; Silvi, S.; Stoddart, J. F. *Science* **2004**, *303*, 1845–1849. (c) Fletcher, S. P.; Dumur, F.; Pollard, M. M.; Feringa, B. L. *Science* **2005**, *310*, 80–82. (d) Qu, D. H.; Wang, Q. C.; Tian, H. *Angew. Chem., Int. Ed.* **2005**, *44*, 5296–5299. (e) Balzani, V.; Clemente-Leon, M.; Credi, A.; Ferrer, B.; Venturi, M.; Flood, A. H.; Stoddart, J. F. *Proc. Natl. Acad. Sci. U.S.A.* **2006**, *103*, 1178–1183. (f) Sindelar, V.; Silvi, S.; Kaifer, A. E. *Chem. Commun.* **2006**, 2185–2187. (g) Serreli, V.; Lee, C.-F.; Kay, E. R.; Leigh, D. A. *Nature* **2007**, *445*, 523–527. (h) Klok, M.; Boyle, N.; Pryce, M. T.; Meetsma, A.; Browne, W. R.; Feringa, B. L. *J. Am. Chem. Soc.* **2008**, *130*, 10484–10485. (i) Zhang, H. Y.; Wang, Q. C.; Liu, M. H.; Ma, X.; Tian, H. *Org. Lett.* **2009**, *11*, 3234–3237. (j) Durola, F.; Lux, J.; Sauvage, J.-P. *Chem.—Eur. J.* **2009**, *15*, 4124–4134.

(10) Silvi, S.; Venturi, M.; Credi, A. *J. Mater. Chem.* **2009**, *19*, 2279–2294.

(11) (a) Collier, C. P.; Mattersteig, G.; Wong, E. W.; Luo, Y.; Beverly, K.; Sampaio, J.; Raymo, F. M.; Stoddart, J. F.; Heath, J. R. *Science* **2000**, *289*, 1172–1175. (b) Luo, Y.; Collier, C. P.; Jeppesen, J. O.; Nielsen, K. A.; DeIonno, E.; Ho, G.; Perkins, J.; Tseng, H.-R.; Yamamoto, T.; Stoddart, J. F.; Heath, J. R. *ChemPhysChem* **2002**, *3*, 519–525. (c) Flood, A. H.; Stoddart, J. F.; Steuerman, D. W.; Heath, J. F. *Science* **2004**, *306*, 2055–2056. (d) Green, J. E.; Choi, J. W.; Boukai, A.; Bunimovich, Y.; Johnston-Halperin, E.; DeIonno, E.; Luo, Y.; Sheriff, B. A.; Xu, K.; Shin, Y. S.; Tseng, H.-R.; Stoddart, J. F.; Heath, J. R. *Nature* **2007**, *445*, 414–417.

(12) (a) Cavallini, M.; Biscarini, F.; Leon, S.; Zerbetto, F.; Bottari, G.; Leigh, D. A. *Science* **2003**, *299*, 531–531. (b) Leigh, D. A.; Morales, M. A. F.; Perez, E. M.; Wong, J. K. Y.; Saiz, C. G.; Slawin, A. M. Z.; Carmichael, A. J.; Haddleton, D. M.; Brouwer, A. M.; Buma, W. J.; Wurpel, G. W. H.; Leon, S.; Zerbetto, F. *Angew. Chem., Int. Ed.* **2005**, *44*, 3062–3067. (c) Berna, J.; Leigh, D. A.; Lubomska, M.; Mendoza, S. M.; Perez, E. M.; Rudolf, P.; Teobaldi, G.; Zerbetto, F. *Nat. Mater.* **2005**, *4*, 704–710.

(13) (a) Nguyen, T. D.; Tseng, H.-R.; Celestre, P. C.; Flood, A. H.; Liu, Y.; Zink, J. I.; Stoddart, J. F. *Proc. Natl. Acad. Sci. U.S.A.* **2005**, *102*, 10029–10034. (b) Nguyen, T. D.; Liu, Y.; Saha, S.; Leung, K. C.-F.; Stoddart, J. F.; Zink, J. I. *J. Am. Chem. Soc.* **2007**, *129*, 626–634. (c) Angelos, S.; Yang, Y.-W.; Khashab, N. M.; Stoddart, J. F.; Zink, J. I. *J. Am. Chem. Soc.* **2009**, *131*, 11344–11345.

(14) (a) Huang, T. J.; Brough, B.; Ho, C.-M.; Liu, Y.; Flood, A. H.; Bonvallet, P. A.; Vignon, S. A.; Tseng, H.-R.; Stoddart, J. F.; Baller, M.; Magonov, S. *Appl. Phys. Lett.* **2004**, *85*, 5391–5393. (b) Liu, Y.; Flood, A. H.; Bonvallet, P. A.; Vignon, S. A.; Northrop, B. H.; Tseng, H.-R.; Jeppesen, J. O.; Huang, T. J.; Brough, B.; Baller, M.; Magonov, S.; Solares, S. D.; Goddard, W. A.; Ho, C.-M.; Stoddart, J. F. *J. Am. Chem. Soc.* **2005**, *127*, 9745–9759. (c) Juluri, B. K.; Kumar, A. S.; Liu, Y.; Ye, T.; Yang, Y.-W.; Flood, A. H.; Fang, L.; Stoddart, J. F.; Weiss, P. S.; Huang, T. J. *ACS Nano* **2009**, *3*, 291–300.

(15) For examples of desymmetrized [2]catenanes with various degrees of control on translational selectivity, see: (a) Livoreil, A.; Dietrich-Buchecker, C. O.; Sauvage, J.-P. *J. Am. Chem. Soc.* **1994**, *116*, 9399–9400. (b) Ashton, P. R.; Perez-Garcia, L.; Stoddart, J. F.; White, A. J. P.; Williams, D. J. *Angew. Chem., Int. Ed. Engl.* **1995**, *34*, 571–574. (c) Ashton, P. R.; Ballardini, R.; Balzani, V.; Credi, A.; Gandolfi, M. T.; Menzer, S.; Perez-Garcia, L.; Prodi, L.; Stoddart, J. F.; Venturi, M.; White, A. J. P.; Williams, D. J. *J. Am. Chem. Soc.* **1995**, *117*, 11171–11197. (d) Baumann, F.; Livoreil, A.; Kaim, W.; Sauvage, J.-P. *Chem. Commun.* **1997**, 35–36. (e) Livoreil, A.; Sauvage, J.-P.; Armaroli, N.; Balzani, V.; Flamigni, L.; Ventura, B. *J. Am. Chem. Soc.* **1997**, *119*, 12114–12124. (f) Asakawa, M.; Ashton, P. R.; Balzani, V.; Credi, A.; Hamers, C.; Mattersteig, G.; Montalti, M.; Shipway, A. N.; Spencer, N.; Stoddart, J. F.; Tolley, M. S.; Venturi, M.; White, A. J. P.; Williams, D. J. *Angew. Chem., Int. Ed.* **1998**, *37*, 333–337. (g) Balzani, V.; Credi, A.; Langford, S. J.; Raymo, F. M.; Stoddart, J. F.; Venturi, M. *J. Am. Chem. Soc.* **2000**, *122*, 3542–3543. (h) Ashton, P. R.; Baldoni, V.; Balzani, V.; Credi, A.; Hoffmann, H. D. A.; Martinez-Diaz, M. V.; Raymo, F. M.; Stoddart, J. F.; Venturi, M. *Chem.—Eur. J.* **2001**, *7*, 3482–3493. (i) Tseng, H.-R.; Vignon, S. A.; Celestre, P. C.; Stoddart, J. F.; White, A. J. P.; Williams, D. J. *Chem.—Eur. J.* **2003**, *9*, 543–556. (j) Leigh, D. A.; Wong, J. K. Y.; Dehez, F.; Zerbetto, F. *Nature* **2003**, *424*, 174–179. (k) Mobian, P.; Kern, J.-M.; Sauvage, J.-P. *Angew. Chem., Int. Ed.* **2004**, *43*, 2392–2395. (l) Hernandez, J. V.; Kay, E. R.; Leigh, D. A. *Science* **2004**, *306*, 1532–1537. (m) Halterman, R. L.; Martyn, D. E. *J. Org. Chem.* **2007**, *72*, 7841–7848.

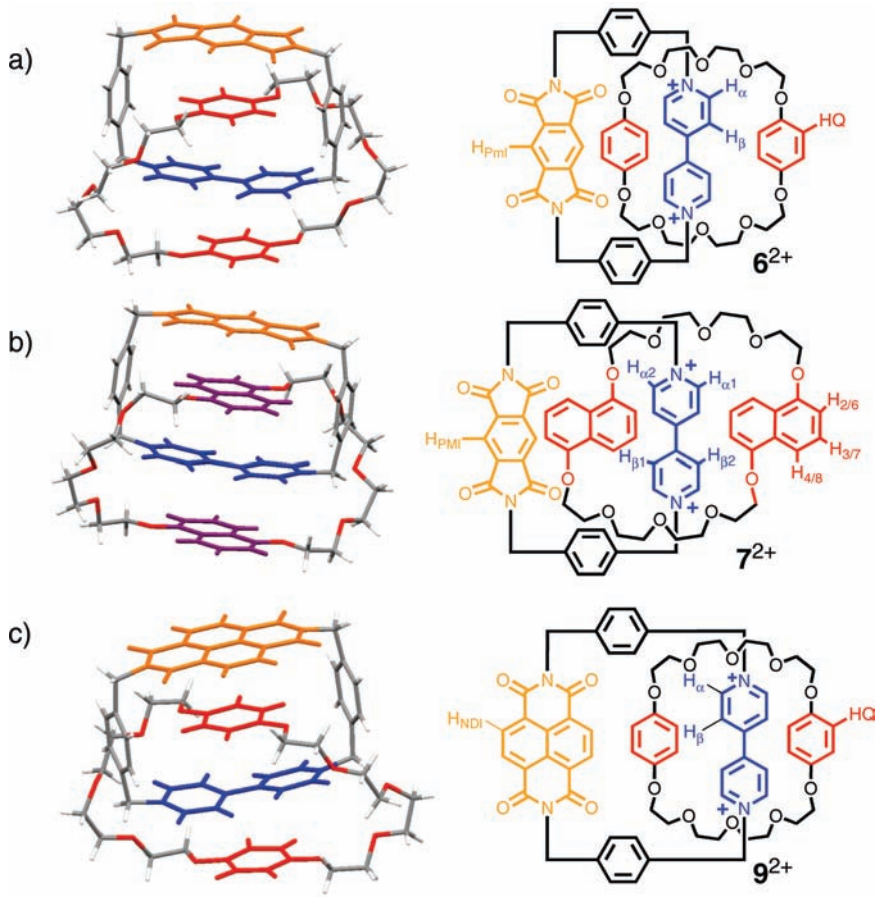


***Figure 1.*** Stick representation of the solid-state structures and the structural formulas of (a) **6**•2$PF_6$, (b) **7**•2$PF_6$, and (c) **9**•2$PF_6$. Solvent molecules and anions are omitted for clarity.

stabilizing [$\pi-\pi$] stacking interactions. In both [2]catenanes, the two pyridinium rings are twisted with an angle of around 10° and the distance between the two quaternary $N^+$ centers is 7.0 Å. The PMI units are not strictly coplanar, with a dihedral angle between the mean planes of the diimide rings of 8 and 5°, and a distance between the two N atoms of PMI units as 6.70 and 6.75 Å, respectively. Various [C−H···O] and [C−H···$\pi$] interactions are present in both [2]catenanes. Intermolecular packings along the axes of the donor−acceptor stacks are present in both cases.

The solid-state structure of NDI-containing [2]catenane **9**•2$PF_6$ implies (Figure 1c) the same common features as the PMI-containing counterpart where the electronically complementary $\pi$-systems are nearly parallel-aligned within two interlocking macrocycles with an interplanar distance around 3.4 Å. Only one translational isomer is observed, in which the $BPY^{2+}$ unit is sandwiched between the two electron-rich moieties of the crown ether. The NDI unit is almost perfectly flat, stacking alongside of the inside HQ unit. The pyridinium rings are twisted with a dihedral angle of 15°. Various [C−H···O] and [C−H···$\pi$] interactions, as well as intermolecular packing along the axes of the donor−acceptor stacks, are observed.

X-ray structural analyses of **8**•2$PF_6$ and **11**•2$PF_6$ reveal the presence of only one translational *co*-conformation out of four possible ones in the solid state. Figure 2 shows that the donors and acceptors arrange alternatively in **8**•2$PF_6$ and **11**•2$PF_6$ in the PMI-TTF-$BPY^{2+}$-DNP and NDI-TTF-$BPY^{2+}$-DNP stacks, respectively, the mean plane of which are parallel with one another with an interplane distance around 3.4 Å. The TTF unit in **8**•2$PF_6$ is bent significantly, with a dihedral angle as high as 25° between the two planes defined by the two thione five-membered rings. In com-

(16) (a) Hamilton, D. G.; Sanders, J. K. M.; Davies, J. E.; Clegg, W.; Teat, S. J. *Chem. Commun.* **1997**, 897–898. (b) Hamilton, D. G.; Davies, J. E.; Prodi, L.; Sanders, J. K. M. *Chem.—Eur. J.* **1998**, *4*, 608–617. (c) Hamilton, D. G.; Montalti, M.; Prodi, L.; Fontani, M.; Zanello, P.; Sanders, J. K. M. *Chem.—Eur. J.* **2000**, *6*, 608–617. (d) Hansen, J. G.; Feeder, N.; Hamilton, D. G.; Gunter, M. J.; Becher, J.; Sanders, J. K. M. *Org. Lett.* **2000**, *2*, 449–452. (e) Iijima, T.; Vignon, S. A.; Tseng, H.-R.; Jarrossson, T.; Sanders, J. K. M; Marchioni, F.; Venturi, M.; Apostoli, E.; Balzani, V.; Stoddart, J. F. *Chem.—Eur. J.* **2004**, *10*, 6375–6392. (f) Kaiser, G.; Jarrosson, T.; Otto, S.; Ng, Y.-F.; Bond, A. D.; Sanders, J. K. M. *Angew. Chem., Int. Ed.* **2004**, *116*, 1993–1996. (g) Vignon, S. A.; Jarrosson, T.; Iijima, T.; Tseng, H.-R.; Sanders, J. K. M.; Stoddart, J. F. *J. Am. Chem. Soc.* **2004**, *126*, 9884–9885. (h) Pascu, S. I.; Jarrosson, T.; Naumann, C.; Otto, S.; Kaiser, G.; Sanders, J. K. M. *New J. Chem.* **2005**, *29*, 80–89. (i) Pascu, S. I.; Naumann, C.; Kaiser, G.; Bond, A. D.; Sanders, J. K. M.; Jarrosson, T. *Dalton Trans.* **2007**, *35*, 3874–3884. (j) Koshkakaryan, G.; Parimal, K.; He, J.; Zhang, X.; Abliz, Z.; Flood, A. H.; Liu, Y. *Chem.—Eur. J.* **2008**, *14*, 10211–10218. (k) Bhosale, S. V.; Jani, C. H.; Langford, S. J. *Chem. Soc. Rev.* **2008**, *37*, 331–342. (l) Au-Yeung, H. Y.; Pantos, D. G.; Sanders, J. K. M. *Proc. Natl. Acad. Sci. U.S.A.* **2009**, *106*, 10466–10470. (m) Koshkakaryan, G.; Klivansky, L. M.; Cao, D.; Snauko, M.; Teat, S. J.; Struppe, J. O.; Liu, Y. *J. Am. Chem. Soc.* **2009**, *131*, 2078–2079.
(17) Liu, Y.; Klivansky, L. M.; Zhang, X. *Org. Lett.* **2007**, *9*, 2577–2580.

(18) It should be noted that the NDI dibromide used for clipping reaction is mixed with impurities resulted from decomposition under the acidic bromination conditions and cannot be purified due to limited solubility. These impurities, together with the poorer solubility of NDI dibromide **2**, are probably responsible for lower yields than the corresponding PMI derivatives.
(19) Crystals suitable for X-ray single crystal analysis were obtained after diffusion of ether into a $Me_2CO$ solution or from a MeCN solution after diffusion of diisopropyl ether. For more crystallographic information, see the crystallographic information files in Supporting Information.

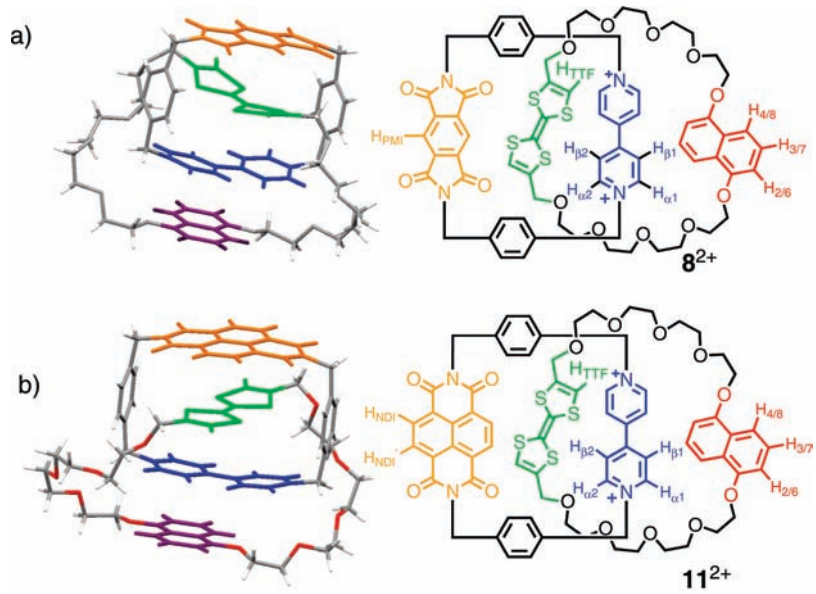


***Figure 2.*** Stick representation of the solid-state structures and the structural formulas of (a) **8**•2$PF_6$ and (b) **11**•2$PF_6$. Solvent molecules and anions are omitted for clarity.

parison, the bending of the TTF unit in **11**•2$PF_6$ is only 8°. Only *trans*-TTF groups are observed in the solid structure in both cases. The PMI and NDI units in individual [2]catenane are slightly bent, with a dihedral angle around 8° and 10°, respectively. In addition, various [C−H···O] and [C−H···$\pi$] interactions as well as extended packing along the stacking direction are present in the solid state structures.

**Translational Selectivity by $^1$H NMR Spectroscopy.** $^1$H NMR spectroscopy provided insightful information for the interlocked structures of these [2]catenanes as well as the *co*-conformation selectivity. For the PMI containing [2]catenanes, the resonances of spectra of **6**•2$PF_6$ or **7**•2$PF_6$ are assignable to one single translational isomer. The "inside" and "outside" HQ or DNP moieties in **6**•2$PF_6$ or **7**•2$PF_6$ are (Figure 3) clearly discernible, suggesting that the site exchange of the two HQ or DNP units is slow at the $^1$H NMR time scale. Two singlets at $\delta$ 6.26 and 3.80 ppm in the spectrum of **6**•2$PF_6$ can be assigned to the "inside" and "outside" HQ, respectively. In the case of **7**•2$PF_6$, the resonances of the two DNP units are expressed in the usual doublet-triplet-doublet coupling pattern. Characteristically, the $H_{4/8}$ of the inside DNP moiety appears as a doublet at $\delta$ 2.95 ppm (inset in Figure 3c) as a result of shielding effect from the nearby dicationic cyclophane. In contrast to **6**•2$PF_6$, all except the PMI protons of the dicationic cyclophane in **7**•2$PF_6$ become diastereotopic. The chemical unequivalence occurs as a result of the local $c_2$ symmetry imposed by the DNP unit on the dicationic cyclophane.

The observation of only one single set of resonances in both **6**•2$PF_6$ and **7**•2$PF_6$ at 297 K suggests that one translational isomer is dominant at this temperature, but it cannot be excluded that the two isomers undergo fast exchange such that only an averaged spectrum is observed. To verify that, the temperature is further lowered to 193 K, at which point the site exchange is slow enough[20] to capture possible translational isomers in equilibrium. As shown in Figure 3b and d, all the peaks of **6**•2$PF_6$ and **7**•2$PF_6$ remain sharp in $CD_3COCD_3$ and no new peaks are observed, suggesting that the single resonance is not a result of site exchange and indeed the translational selectivity is maintained throughout. On the basis of the detection limit of $^1$H NMR spectroscopy, a selectivity greater than 97:3 can be estimated for both [2]catenanes.

Upon replacing the PMI unit with a more electron deficient $\pi$-acceptor, the translational selectivity is maintained, as revealed by the presence of only one single isomer in the $^1$H NMR spectra of both NDI-containing [2]catenanes **9**•2$PF_6$ and **10**•2$PF_6$ (Figure 4). The symmetry of the crown ethers is broken owing to catenation and slow site exchange, resulting in two sets of HQ or DNP protons in **9**•2$PF_6$ or **10**•2$PF_6$. The "inside" and "outside" HQ protons of **9**•2$PF_6$ resonate as two singlets at $\delta$ 6.25 and 3.55, respectively. In the case of **10**•2$PF_6$, two groups of doublet-triplet-doublet are assignable to the resonances of the two DNP units. A characteristic doublet at $\delta$ 2.98 ppm is observed, corresponding to the $H_{4/8}$ of the inside DNP moiety. The NDI protons of the dicationic cyclophane in **9**•2$PF_6$ appear as a singlet at 8.43 ppm. In the case of **10**•2$PF_6$, *ortho* coupling of the aromatic protons of the NDI unit results in two doublets at $\delta$ 8.04 and 7.78 ppm. This splitting, together with the diastereotopic splitting of all other protons of the dicationic cyclophane in **10**•2$PF_6$, is consistent with the local $c_2$ symmetry imposed by the DNP unit. Variable temperature studies indicate[21] that no new resonances corresponding to other isomers are observed throughout the temperature range from 193 to 298 K, consistent with the crown ether ring component located selectively on the $BPY^{2+}$ unit. The translational selectivity is thus preserved in these NDI derived [2]catenanes.

The combination of two different donors and two different acceptors in [2]catenanes **8**•2$PF_6$ and **11**•2$PF_6$ leads to four possible translational isomers. This situation can be further complicated when taking account of *cis/trans* positional isomers of the TTF group, which coexist in the starting crown ether **5** in a ratio of 2:3. Despite the complexity of the systems, the well-resolved $^1$H NMR spectra indicate the presence of only one isomer, suggesting a remarkable

(20) Two mechanisms are possible for the exchange between the two translational isomers. Either the dicationic cyclophane rotates through the center of the crown ether component, or the outer DNP unit can sweep round the dicationic cyclophane by pirouetting about the included DNP moiety. According to studies by the Stoddart group on structurally similar [2]catenanes, (see: Stoddart, J. F; et al. *J. Am. Chem. Soc.* **1992**, *114*, 193–218. ) the latter one is the lower energy process as it requires least energy for the breakdown of donor-acceptor interactions. The typical associated activation barrier for Stoddart's systems is around 12−14 kcal $mol^{-1}$. Correspondingly, those site exchange processes can be efficiently "frozen out" below 243 K. For compounds **6**•2$PF_6$ and **7**•2$PF_6$, such activation barrier is difficult to measure on account of the absence of other isomers. However, they should be very similar to those reported systems, both of which involve the breaking of donor-acceptor interactions between $BPY^{2+}$ and the outer aromatic units.

(21) See Supporting Information.

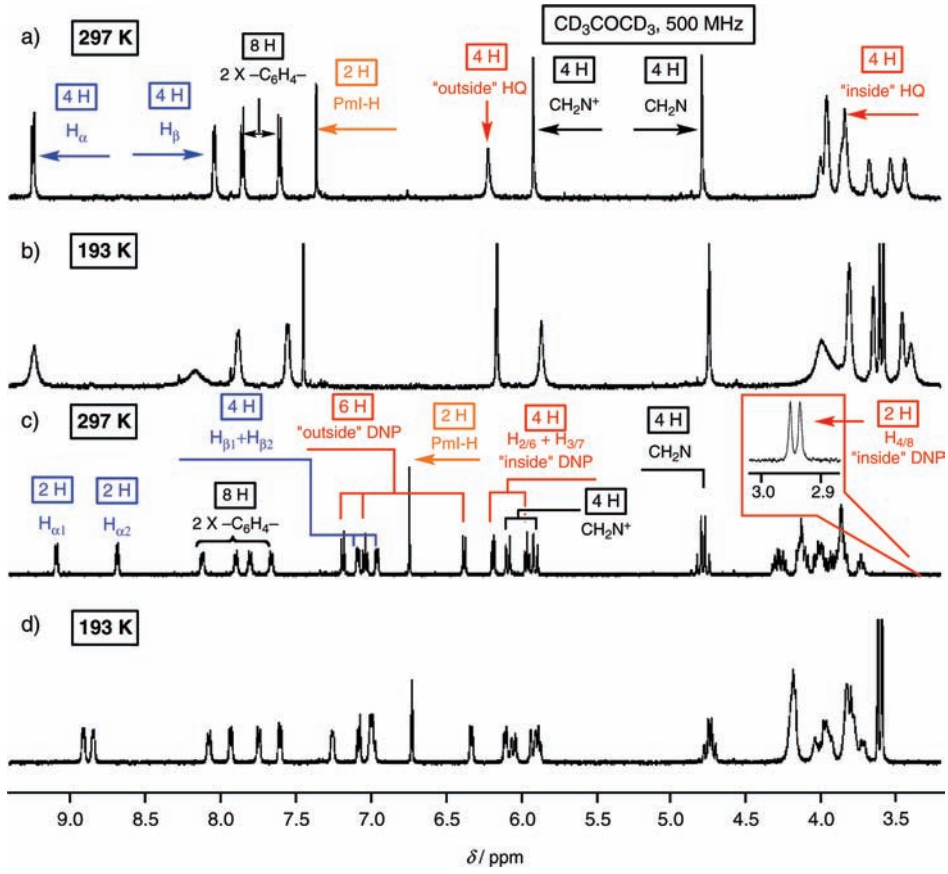


***Figure 3.*** Partial $^1$H NMR spectra of (a) **6**•2PF$_6$ at 297 K, (b) **6**•2PF$_6$ at 193 K, (c) **7**•2PF$_6$ at 297 K, and (d) **7**•2PF$_6$ at 193 K. The inset in c shows the doublet corresponding to $H_{4/8}$ of the inside DNP unit.

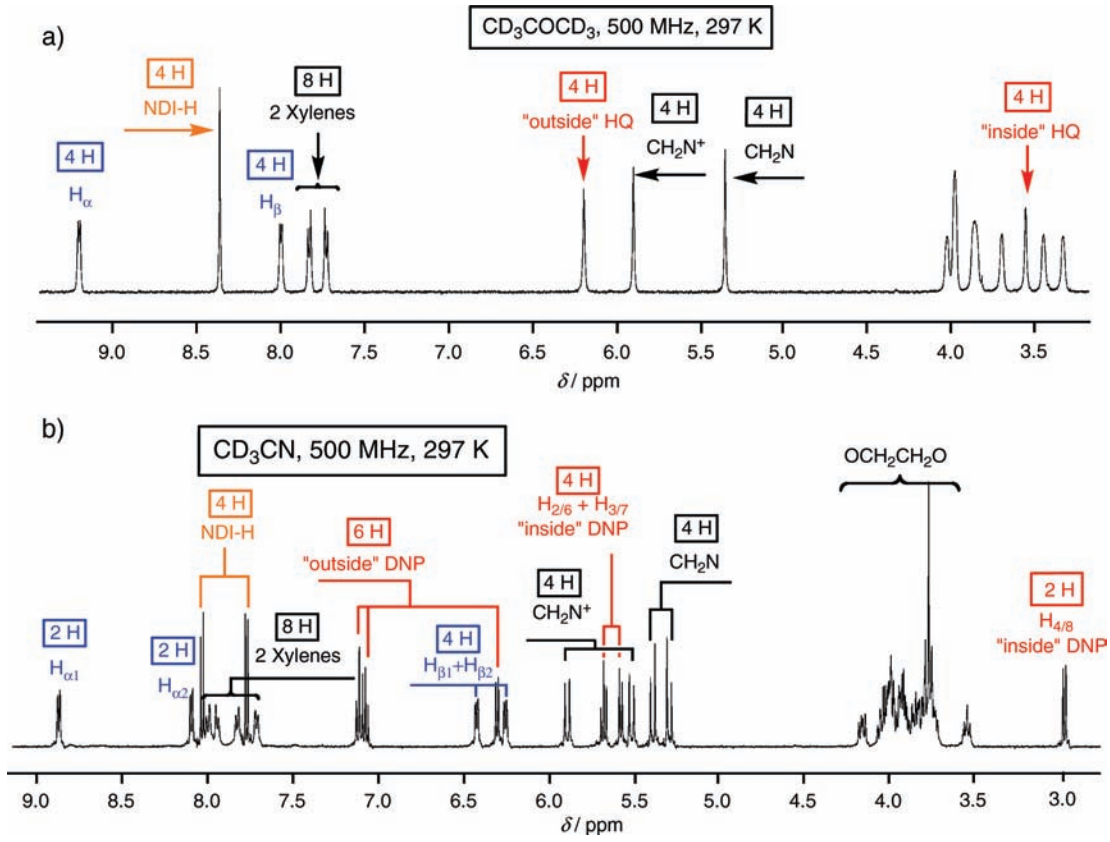


***Figure 4.*** Partial $^1$H NMR spectra of (a) **9**•2PF$_6$ and (b) **10**•2PF$_6$.

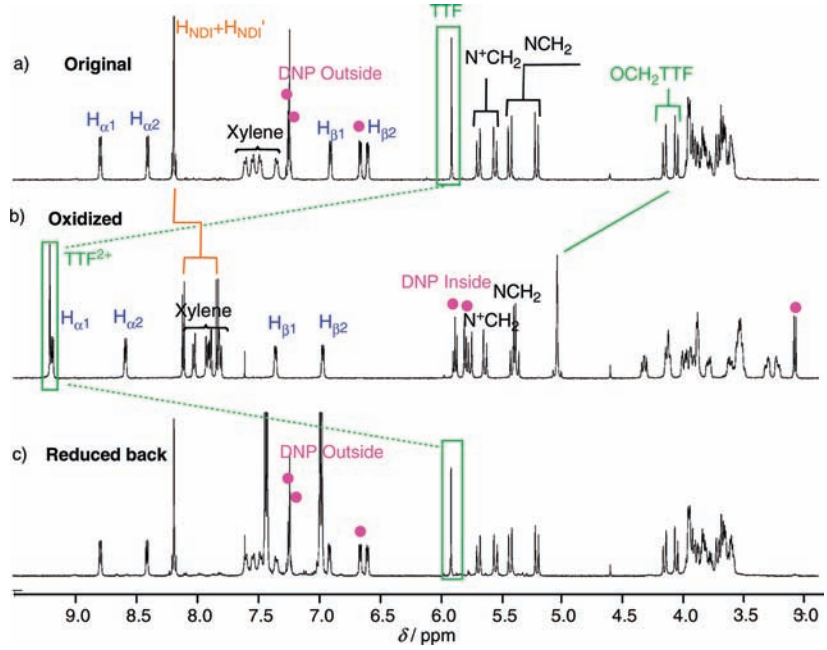


***Figure 5.*** $^1$H NMR spectra of [2]catenane **11**•2PF$_6$ (273 K, $CD_3CN$, 500 MHz) (a) before the addition of oxidant, (b) after the addition of 2.2 equiv oxidant, and (c) after the addition of Zn powder.

translational selectivity and the absence of *cis/trans* TTF isomerization. The only TTF positional isomer can be assigned to the *trans* one, which is more electronically and/or sterically favored in the catenated structure, as is confirmed by the X-ray structures. As indicated in the $^1$H NMR spectrum of **11**•2PF$_6$ (Figure 5a), the TTF protons resonate at 5.95 ppm as a singlet while the DNP protons display the usual doublet-triplet-doublet coupling pattern at the aromatic region. The lack of a doublet at the high field region around $\delta$ 3.0 ppm confirms the location of DNP being outside of the cyclophane. The protons of the cyclophane component became diastereotopic, in agreement with the symmetry breakdown by the DNP unit. The translational selectivity is preserved as verified by variable temperature $^1$H NMR spectroscopic studies.[21] Similarly, the $^1$H NMR spectra of **8**•2PF$_6$ displays spectroscopic features consistent with the exclusive translational and positional selectivity.[21]

**Chemical Switching by $^1$H NMR Spectroscopy.** The translocation of crown ether component in the TTF-containing [2]catenanes **8**•2PF$_6$ and **11**•2PF$_6$ can be driven chemically, as monitored by $^1$H NMR spectroscopy in an oxidation−reduction cycle. During the oxidation of **11**•2PF$_6$ using 2.2 equiv. oxidant, tris(4-bromophenyl)iminium hexachloroantimonate, the TTF singlet shifts (Figure 5b) downfield by more than 3 ppm, in accordance with the formation of $TTF^{2+}$. Commensurate with the oxidation process, pronounced chemical shift changes are observed for the DNP protons. A doublet emerges at $\delta$ 2.95 ppm for **11**$^{4+}$, which suggests that the DNP unit is now included in the cyclophane cavity. This translocation of the crown ether component is completely reversible. After the addition of Zn powder and vigorous shaking, the original spectrum is fully restored (Figure 5c).

One remaining question about the oxidative switching is whether the dicationic cyclophanes also undergo circumrotation on account of the increased electrostatic repulsion between $BPY^{2+}$ and the newly formed $TTF^{2+}$ (Scheme 2). An analysis of the spectral changes of NDI protons in **11**•2PF$_6$ reveals (Figure 5a and b) a larger peak separation upon oxidation, indicating a dramatic change of its surrounding chemical environment that can be accounted for by the switch of the stacking partner from TTF to DNP. A comparison of the $^1$H NMR spectra of **10**$^{2+}$ and the oxidized **11**$^{4+}$ indicates (Table 1) that the NDI protons display very similar chemical shifts and splitting pattern, suggesting a similar chemical environment in both molecules. This similarity implies that no translocation of the dicationic cyclophane occurs in response to the oxidative switching of **11**$^{2+}$ and the NDI unit remains outside of the electron-rich crown ether, despite the increased charge repulsion between $BPY^{2+}$ and the $TTF^{2+}$. Presumably the polyethylene glycol chains in the crown ether provide sufficient flexibility for the $TTF^{2+}$ group to oscillate around to keep a distance from the $BPY^{2+}$ unit to minimize charge−charge repulsion.

***Table 1.*** Comparison of the $^1$H NMR Chemical Shift Data of **7**$^{2+}$ vs the Oxidized **8**$^{4+}$, and **10**$^{2+}$ vs the Oxidized **11**$^{4+}$ (500 MHz, 273 K, $CD_3CN$)[a]

| compound | $H_{PMI}$ | $H_{NDI}$ |
|---|---|---|
| **7**$^{2+}$ | 6.76 | − |
| **8**$^{4+}$ | 6.88 (0.12) | − |
| **10**$^{2+}$ | − | 8.03, 7.77 |
| **11**$^{4+}$ | − | 8.11 (0.08), 7.83 (0.06) |

[a] Number in parentheses indicates chemical shift changes.

The oxidation−reduction experiment on **8**•2PF$_6$ disclosed similar switching behavior, as evidenced by $^1$H NMR spectroscopy.[21] The characteristic chemical shift changes associated with the TTF and DNP units indicated that upon two-electron oxidation, the $TTF^{2+}$ is dislocated outside of the cavity of the dicationic cyclophane while DNP is now encircled. By comparing the $^1$H NMR spectra of **7**$^{2+}$ and the oxidized **8**$^{4+}$ (Table 1), it is concluded that the PMI stays outside of the crown ether cavity in response to the double oxidation of the TTF unit.

The successful oxidative switching of the electron donors prompts us to conduct a chemical switching by reduction of the electron acceptors. Sodium hydrosulfite is used as the reducing agent, which is shown to effectively reduce the $BPY^{2+}$ unit in [2]catenane **6**•2PF$_6$ to give a blue color as a result of the formation of $BPY^{+}$ radical cation. The paramagnetic nature of the generated radical cation, however, leads to a very broad spectrum which prevents a meaningful $^1$H NMR spectroscopic analysis.

**Photophysical Properties.** The photophysical properties of [2]catenanes **6**$^{2+}$−**11**$^{2+}$ are investigated and compared against a number of model compounds (Scheme 3). Compounds **12**−**13** are synthesized[21] and studied under similar conditions as for the [2]catenanes. The physicochemical data for the previously studied [2]catenanes **15**$^{4+}$−**17**$^{4+}$ and **18**−**19**[15c,16b,c] are reported for comparison purposes. Compounds **12** and **13** exhibit the absorption

***Scheme 2.*** Illustration of Circumrotation of the Molecular Components during the Oxidative Switch of $\mathbf{11}^{2+}$

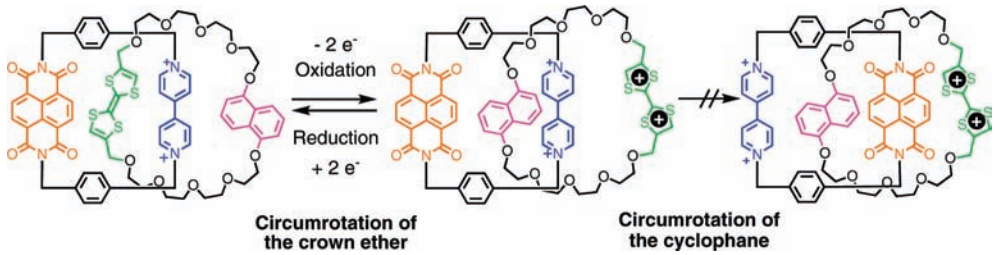


***Scheme 3.*** Structural Formulas of Model Compounds

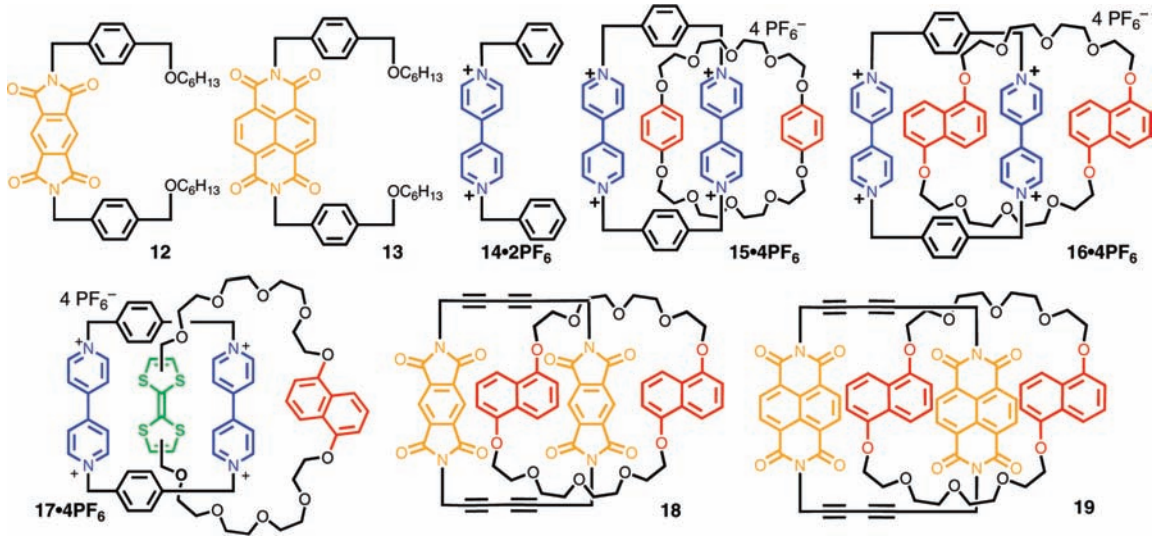


bands expected for their PMI[22] and NDI[23] moieties, respectively, and no luminescence. Compound $\mathbf{14}^{2+}$ shows the typical absorption band of the $BPY^{2+}$ unit[24] and no luminescence.[25] The crown ether rings **3** and **4** exhibit an absorption band in the near-UV region and an intense fluorescence emission ($\lambda_{max}$ = 324 and 345 nm, respectively) ascribed to their HQ or DNP units, respectively, in agreement with previous investigations.[15c] The absorption spectrum of macrocycle **5** is that expected on the basis of its TTF and DNP chromophoric units.[15f,26] The DNP emission in **5** is strongly quenched (>100 times weaker compared with that of **4**), presumably because of an electron-transfer process from the TTF moiety to the excited DNP unit.

The absorption spectra of [2]catenanes $\mathbf{6}^{2+}$−$\mathbf{11}^{2+}$ are different from the sum of the spectra of the respective chromophoric components (Table 2). As shown for $\mathbf{10}^{2+}$ (Figure 6), a considerable decrease in the intensity of the UV absorption of its chromophoric units and a blurring of the vibrational structure of the DNP and NDI bands are observed. Additionally, all [2]catenanes exhibit (Table 2 and Figure 7) a weak and broad band in the visible region assigned to the charge-transfer (CT) interaction between the $\pi$-acceptor and $\pi$-donor units incorporated in the molecular components.

The discussion of the CT bands in these [2]catenanes is particularly interesting because, in principle, different interactions can occur, depending on the types of donor and acceptor units engaged. Only one CT band is observed in the absorption spectrum of either $\mathbf{6}^{2+}$ or $\mathbf{7}^{2+}$, which is very similar to that shown by the respective tetracationic cyclobisparaquat-based model compounds $\mathbf{15}^{4+}$ or $\mathbf{16}^{4+}$. This result is consistent with the *co*-conformation of $\mathbf{6}^{2+}$ and $\mathbf{7}^{2+}$, in which the BPP34C10 or DNP38C10 macrocyclic component encircles the better electron accepting $BPY^{2+}$ unit. On the other hand, the CT band arising from the interaction between the electron donors and the alongside electron acceptors, such as DNP and PMI pair in $\mathbf{7}^{2+}$, expected at around 460 nm on the basis of the results obtained for the model compound **18** ($\lambda_{max}$ = 455 nm and $\varepsilon$ = 730 $M^{-1}$ $cm^{-1}$ in $CH_2Cl_2$),[16b] is not observed (Figure 7). For $\mathbf{8}^{2+}$ in its stable *co*-conformation three different CT interactions can be expected, involving (i) TTF−$BPY^{2+}$, (ii) TTF−PMI, and (iii) DNP−$BPY^{2+}$ units, respectively. Also in this case, however, only one CT band with $\lambda_{max}$ = 800 nm and $\varepsilon$ = 3600 $M^{-1}$ $cm^{-1}$ (Figure 7) is observed, which is consistent with the TTF group interacting with the $BPY^{2+}$ unit of the cyclophane (for $\mathbf{17}^{4+}$ $\lambda_{max}$ = 835 nm and $\varepsilon$ = 3500 $M^{-1}$ $cm^{-1}$).[15f,27,28] The CT band for the DNP−$BPY^{2+}$ interaction, expected at around 530 nm as seen in the model compound $\mathbf{16}^{4+}$ ($\lambda_{max}$ = 529 nm and $\varepsilon$ = 1100 $M^{-1}$ $cm^{-1}$),[15c] is absent, in agreement with previous observations on related [2]catenanes.[26] No CT band in the region between 450 and 800 nm is observed, suggesting the lack of meaningful

(22) Wiederrecht, G. P.; Niemczyk, M. P.; Svec, W. A.; Wasielewski, M. R. *J. Am. Chem. Soc.* **1996**, *118*, 81–88.
(23) (a) Sazanovich, I. V.; Alamiry, M. H.; Best, J.; Bennett, R. D.; Bouganov, O. V.; Davies, E. S.; Grivin, V. P.; Meijer, A. J. H. M.; Plyusnin, V. F.; Ronayne, K. L.; Shelton, A. H.; Tikhomirov, S. A.; Towrie, M.; Weinstein, J. A. *Inorg. Chem.* **2008**, *47*, 10432–10445. (b) Rogers, J. E.; Kelly, L. A. *J. Am. Chem. Soc.* **1999**, *121*, 3854–3861. (c) Demeter, A.; Brces, T.; Biczk, L.; Wintgens, V.; Valat, P.; Kossanyi, J. *J. Phys. Chem.* **1996**, *100*, 2001–2011.
(24) Monk, P. M. S. *The Viologens: Physicochemical Properties, Synthesis and Applications of the Salts of 4,4′-Bipyridine*; Wiley: New York, 1998.
(25) Ballardini, R.; Credi, A.; Gandolfi, M. T.; Giansante, C.; Marconi, G.; Silvi, S.; Venturi, M. *Inorg. Chim. Acta* **2007**, *360*, 1072–1082.
(26) Balzani, V.; Credi, A.; Mattersteig, G.; Matthews, O. A.; Raymo, F. M.; Stoddart, J. F.; Venturi, M.; White, A. J. P.; Williams, D. J. *J. Org. Chem.* **2000**, *65*, 1924–1936.
(27) Witlicki, E. H.; Hanses, S. W.; Christensen, M.; Hansen, T. S.; Nygaard, S. D.; Jeppesen, J. O.; Wong, E. W.; Jensen, L.; Flood, A. H. *J. Phys. Chem. A* **2009**, *113*, 9450–9457.

***Table 2.*** UV−vis Absorption and Luminescence Properties of the Investigated Catenanes and Model Compounds (Air Equilibrated $CH_3CN$, Room Temperature)

| | absorption | | | | luminescence | | |
|---|---|---|---|---|---|---|---|
| compound | $\lambda_{max}$ (nm) | $\varepsilon_{max}$ (L mol$^{-1}$ cm$^{-1}$) | $\Delta\nu_{1/2}^{CT}$(cm$^{-1}$)[a] | $H_{DA}$ (cm$^{-1}$)[b] | $\lambda_{max}$ (nm) | $\Phi$[c] | $\tau$ (ns) |
| $\mathbf{6}^{2+}$ | 267[d] | 19000 | | | | | |
| | 461 | 530 | 7450 | 1830 | | | |
| $\mathbf{7}^{2+}$ | 275 | 19000 | | | | | |
| | 507 | 800 | 6710 | 2030 | | | |
| $\mathbf{8}^{2+}$ | 283 | 25000 | | | | | |
| | 800 | 3600 | 3930 | 2630 | | | |
| $\mathbf{9}^{2+}$ | 269 | 20000 | | | | | |
| | 382 | 19000 | | | | | |
| | 480 | 700 | 6110 | 1860 | | | |
| $\mathbf{10}^{2+}$ | 274 | 23000 | | | | | |
| | 367 | 12000 | | | | | |
| | 526 | 900 | 5770 | 1960 | | | |
| $\mathbf{11}^{2+}$ | 285 | 23000 | | | | | |
| | 369 | 15000 | | | | | |
| | 815 | 3200 | 3850 | 2430 | | | |
| **3** | 291 | 5100 | | | 324 | 0.10 | 3.0 |
| **4** | 296 | 16100 | | | 345 | 0.35 | 7.1 |
| **5** | 297 | 16700 | | | | | |
| **12** (PMI control)[e] | 319 | 2600 | | | | | |
| **13** (NDI control)[e] | 379 | 27000 | | | | | |
| $\mathbf{14}^{2+}$ (BPY control) | 260 | 20000 | | | | | |

[a] Half-width (fwhm) of the CT absorption band. [b] Donor−acceptor electronic coupling element; see text for details. [c] Luminescence quantum yield. [d] Shoulder. [e] For solubility reasons, the experiments were carried out in $CH_3CN/CHCl_3$ 98:2 (v/v).

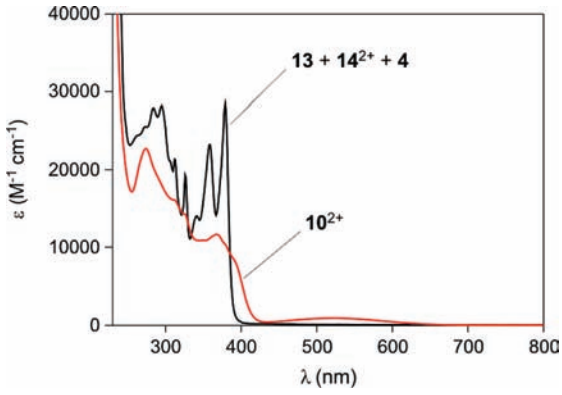


***Figure 6.*** Absorption spectrum of [2]catenane $\mathbf{10}^{2+}$ (red) compared with the sum of the spectra of **13** and $\mathbf{14}^{2+}$, as models for the chromophoric units contained in the $BPY^{2+}$−NDI cyclophane, and of macrocycle **4** (black).

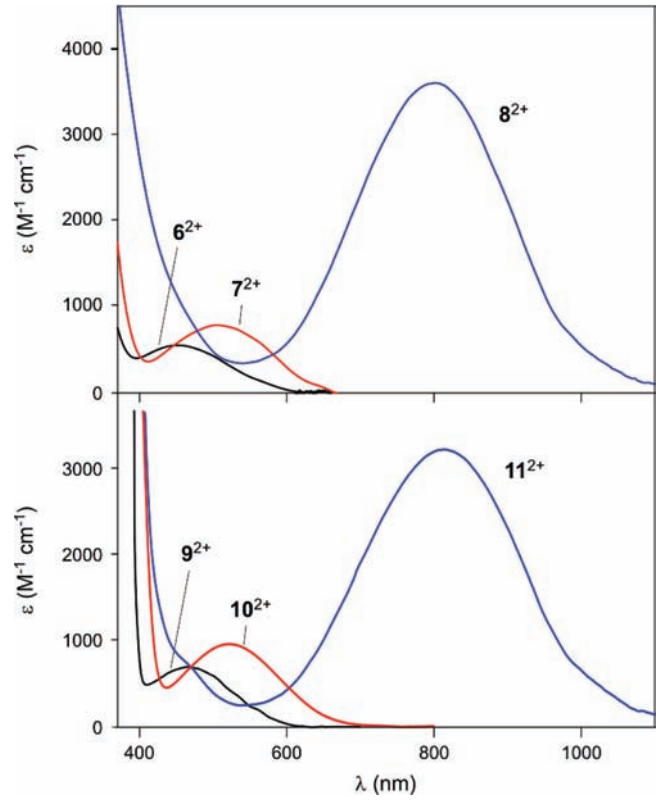


***Figure 7.*** CT absorption bands of the [2]catenanes containing the PMI unit (top) and the NDI unit (bottom).

TTF−PMI interactions. In summary, for the [2]catenanes containing the PMI−$BPY^{2+}$ cyclophane only the charge-transfer interaction involving the better $\pi$-acceptor unit ($BPY^{2+}$)—and, in case of a choice as for $\mathbf{8}^{2+}$, the better $\pi$-donor unit—can be evidenced in the absorption spectra.

The analysis for the [2]catenanes containing the NDI-$BPY^{2+}$ cyclophane is further complicated by the fact that the CT absorption band expected when the NDI unit is involved as the electron acceptor, as revealed in the model compound **19** ($\lambda_{max}$ = 523 nm, $\varepsilon$ = 350 M$^{-1}$ cm$^{-1}$ in $CH_2Cl_2$),[16b] occurs at a wavelength very similar to that of the CT band involving the $BPY^{2+}$ unit.[15c] In any instance, the CT bands of $\mathbf{9}^{2+}$ and $\mathbf{10}^{2+}$ (Figure 7) are very similar to those shown by $\mathbf{6}^{2+}$ and $\mathbf{7}^{2+}$ (or model compound $\mathbf{15}^{4+}$ and $\mathbf{16}^{4+}$), respectively, in agreement with a structure in which BPP34C10 or DNP38C10 encircles the $BPY^{2+}$ electron-accepting unit. The visible absorption spectrum of $\mathbf{11}^{2+}$ is dominated by a band assigned to the CT interaction involving the $BPY^{2+}$ and TTF units ($\lambda_{max}$ = 815 nm, $\varepsilon$ = 3200 M$^{-1}$ cm$^{-1}$);[15f,27,28] a shoulder in the region between 450 and 500 nm ($\varepsilon$ ca. 700 M$^{-1}$ cm$^{-1}$ at 470 nm) is also observed. On the basis of the *co*-conformation of this catenane, and in view of the poorer electron-accepting ability of the NDI unit with respect

(28) It can be noticed that the TTF-$BPY^{2+}$ CT band of catenanes $\mathbf{8}^{2+}$ and $\mathbf{11}^{2+}$ has almost the same molar absorption coefficient as that of model compound $\mathbf{17}^{4+}$, although the former catenanes possess only one $BPY^{2+}$ unit. Indeed, it was recently shown (ref 4g) that the alongside CT interaction between a TTF and a $BPY^{2+}$ units can give rise to a band with an absorption coefficient similar to that of the present catenanes. As observed in previous investigations on related catenanes (refs 15c, g), the CT band intensities in this type of catenanes do not usually scale linearly with the number of donor and acceptor units involved.

***Table 3.*** Electrochemical Data for the [2]Catenanes and Model Compounds ($CH_3CN$, Room Temperature)[a]

| compound | reduction | oxidation | $\lvert\Delta E_{red}\rvert + \lvert\Delta E_{ox}\rvert$ (V) |
|---|---|---|---|
| $\mathbf{6}^{2+}$ | −0.42, −0.85, −0.98, −1.53 | +1.40,[b] +1.58[b] | 0.23 |
| $\mathbf{7}^{2+}$ | −0.54, −0.95,[c] −1.50 | +1.33,[b] +1.50[b] | 0.47 |
| $\mathbf{8}^{2+}$ | −0.50, −0.92,[c] −1.41 | +0.57,[d] +0.76, +1.49[b] | 0.43 |
| $\mathbf{9}^{2+}$ | −0.39, −0.67, −0.96, −1.10 | +1.39,[b] +1.56[b] | 0.19 |
| $\mathbf{10}^{2+}$ | −0.55, −0.73, −0.96, −1.09 | +1.32,[b] +1.46[b] | 0.47 |
| $\mathbf{11}^{2+}$ | −0.51, −0.70, −0.98, −1.10 | +0.59[d], +0.78, +1.49[b] | 0.46 |
| **3** | − | +1.24,[b] +1.37[b] | |
| **4** | − | +1.05,[b] +1.15[b] | |
| **5** | − | +0.29, +0.72, +1.28[b] | |
| **12** (PMI control)[e] | −0.82, −1.39 | − | |
| **13** (NDI control)[e] | −0.58, −1.01 | − | |
| $\mathbf{14}^{2+}$ ($BPY^{2+}$ control)[f] | −0.35, −0.78 | − | |
| $\mathbf{15}^{4+}$[f,g] | −0.31, −0.44, −0.84[c] | +1.42,[b] +1.72[b] | |
| $\mathbf{16}^{4+}$[f] | −0.35, −0.56, −0.81, −0.89 | +1.30,[b,g] +1.55[b,h] | |
| $\mathbf{17}^{4+}$[h,i] | −0.33, −0.49, −0.87[c] | +0.80[c], +1.60[b] | |
| **18**[j] | −0.94, −1.14, −1.57[c] | | |
| **19**[j] | −0.70, −0.98, −1.18[c] | | |

[a] Halfwave potential values of reversible and monoelectronic processes in V vs SCE, unless otherwise noted. Conditions: glassy carbon electrode, tetraethylammonium hexafluorophosphate as supporting electrolyte, ferrocene ($E_{1/2}$ = +0.395 V vs SCE) or decamethylferrocene ($E_{1/2}$ = −0.110 V vs SCE) employed as an internal reference. [b] Irreversible or poorly reversible process; redox potential estimated from the DPV peak recorded at 20 mV/s. [c] Two-electron process. [d] Process characterized by a large separation between the cathodic and anodic peaks; potential taken from DPV measurements at 20 mV/s. [e] For solubility reasons the experiments were carried out in $CH_3CN/CHCl_3$ 9:1 (*v*/*v*). [f] Data from ref 15c. [g] Data from ref 33. [h] Data from ref 15f. [i] Data from ref 26. [j] Data obtained in $CH_2Cl_2$, from ref 16b.

to $BPY^{2+}$, this shoulder can tentatively be ascribed to the CT interaction between the NDI and TTF units.

The features of the CT absorption bands can be related to the electronic coupling element $H_{DA}$ between the donor and acceptor units involved in the charge-transfer transition. Hush showed that in the case of a Gaussian-shaped CT band the donor−acceptor electronic coupling element can be calculated by the following equation:[29,30]

$$H_{DA} = 2.06 \times 10^{-2} \frac{\sqrt{\nu_{max} \varepsilon_{max} \Delta\nu_{1/2}}}{R_{DA}} \quad (1)$$

where $\nu_{max}$ and $\Delta\nu_{1/2}$ are the band maximum and half-width in $cm^{-1}$, $\varepsilon_{max}$ is the molar absorption coefficient at the band maximum in L $mol^{-1}$ $cm^{-1}$, and $R_{DA}$ is the distance separating the donor and acceptor moieties in Å. In these [2]catenanes, the donor−acceptor distance can be unambiguously estimated considering that the electron donating unit is sandwiched into a rigid electron accepting macrocycle; X-ray structural investigations show that $R_{DA}$ is about 3.3 Å (see above). The electronic coupling elements for the investigated [2]catenanes, calculated from eq 1, are compiled in Table 2. It can be noted that [2]catenanes containing the same electron donating ring exhibit nearly identical $H_{DA}$ values, in spite of the fact that they contain different units (PMI or NDI) as the secondary electron acceptor. This observation supports the previous discussion, that is, the CT band originates from an interaction in which $BPY^{2+}$ unit is the prevailing electron acceptor. The value of $H_{DA}$ for [2]catenanes containing different donor moieties increases in the order HQ < DNP ≪ TTF, thereby reflecting the increasing $\pi$-electron donating ability of such units.

None of the examined [2]catenanes exhibited bona fide emission upon excitation either in the UV region or in the visible CT band.[31] Hence, we conclude that the potentially fluorescent singlet excited states localized on the HQ and DNP units undergo radiationless deactivation when these units are contained in the [2]catenanes. It is likely that the deactivation to the lower-lying, nonemissive CT states provides an efficient route for the nonradiative decay of the upper-lying excited states, in line with previous observations on similar systems.[15c,f−h,16a−c,26]

**Electrochemical Experiments.** In the [2]catenanes, the uptake and removal of electrons by the acceptors and from the donors, respectively, can trigger *co*-conformational rearrangements involving the exchange of inside and alongside units through the circumrotation of the molecular components.[15c,f,26,32] This behavior is interesting for the potential utilization of [2]catenanes as electrochemically driven molecular machines.[15a,c−f] Comprehensive electrochemical studies of [2]catenanes $\mathbf{6}^{2+}$−$\mathbf{11}^{2+}$ as well as the model compounds are carried out to probe the *co*-conformational changes in response to electrochemical stimuli.

The electrochemical data for the examined compounds in argon purged $CH_3CN$ solution are gathered in Table 3. All donors and acceptors embedded within the [2]catenane structures are electroactive in the examined potential window (from +2 to −2 V vs saturated calomel electrode, SCE). Crown ethers **3**, **4**, and **5** exhibit oxidation processes and no reduction, as expected on the basis of their HQ, DNP, and TTF units.[15c,f,33] The potential values for the first oxidation (Table 3) suggest that the electron donating ability should increase in the order HQ < DNP ≪ TTF. Compounds **12**, **13**, and $\mathbf{14}^{2+}$, that can be taken as models for the PMI, NDI, and $BPY^{2+}$ units, respectively, show two consecutive monoelectronic and reversible reduction processes and no oxidation. On the basis of the first reduction potential (Table 3), it can be estimated that the electron accepting ability should increase in the order PMI < NDI < $BPY^{2+}$.

The cyclic voltammograms (CVs) of all [2]catenanes exhibit the expected redox processes associated with their electroactive units. As a consequence of intercomponent CT interactions in the catenated structures, the potential values for these processes are shifted (Table 3) in comparison with the model compounds. The discussion of the electrochemical properties of the present desymmetrized [2]catenanes is greatly facilitated by the use of "genetic" diagrams that correlate the potential values observed for the

(29) Hush, N. S. *Prog. Inorg. Chem.* **1967**, *8*, 391–444.
(30) Brunschwig, B. S.; Sutin, N. In *Electron Transfer in Chemistry*; Balzani, V., Ed.; Wiley-VCH: Weinheim, 2001; Vol. II, p 600.
(31) A very weak HQ- or DNP-type fluorescence, whose intensity was from two to three orders of magnitude smaller than that of the crown ethers **3** or **4**, respectively, was detected upon UV excitation. Fluorescence lifetime measurements indicate that such emissions originate from small amounts of strongly emissive impurities.
(32) Kaifer, A. E.; Gomez-Kaifer, M. *Supramolecular Electrochemistry*; Wiley-VCH: Weinheim, 2000.
(33) Ballardini, R.; Balzani, V.; Credi, A.; Brown, C. L.; Gillard, R. E.; Montalti, M.; Philp, D.; Stoddart, J. F.; Venturi, M.; White, A. J. P.; Williams, B. J.; Williams, D. J. *J. Am. Chem. Soc.* **1997**, *119*, 12503–12513.

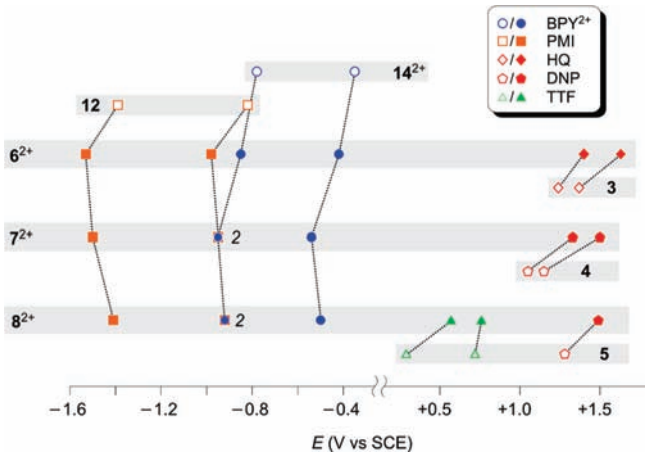


***Figure 8.*** Correlation diagram of the redox potentials of the [2]catenanes containing the PMI electron accepting unit (filled symbols), and of their molecular components and model compounds (empty symbols). Two-electron processes are labeled with the number 2.

[2]catenane with those of appropriate parent compounds. The assignment of each process to the corresponding electroactive unit is thus made by comparison with the behavior of model systems and assisted by spectroelectrochemical experiments. Only reversible processes will be discussed in detail.

**[2]Catenanes Containing the PMI Unit.** CVs of [2]catenanes $\mathbf{6}^{2+}$ and $\mathbf{7}^{2+}$ (Figure 8) show two irreversible oxidative processes associated with the oxidation of the two HQ or DNP units. These processes are positively shifted with respect to the crown ethers as a result of stabilizing CT interactions. The incorporation of two different donors in the [2]catenane $\mathbf{8}^{2+}$ endows rich electrochemical information. Three oxidative processes are observed for $\mathbf{8}^{2+}$ (Figure 9a): the first two (+0.57 V and +0.76 V) are assigned to the two consecutive monoelectronic TTF oxidations,[34] (Figure 9b) while the third one (+1.49 V) is ascribed to the oxidation of the DNP unit. The first TTF oxidation is substantially displaced (280 mV) toward more positive potentials as compared to the free crown ether **5**, in agreement with the fact that TTF occupies the inside position and is strongly involved in CT interactions. This process is characterized by a large separation between the anodic and the cathodic cyclic voltammetric peaks, which are also scan-rate dependent—on increasing the scan rate, the former moves toward more positive potentials and the latter toward less positive potentials. The $TTF^{+/2+}$ oxidation is reversible and occurs at a similar potential compared with the same process in the crown ether **5**, while the oxidation of the DNP unit is strongly displaced toward positive potentials. The scan-rate dependence of the separation between the anodic and cathodic peaks of the $TTF^{0/+}$ process in $\mathbf{8}^{2+}$ indicates that oxidation is followed by a rearrangement taking place on the time scale of the electrochemical experiment, as previously observed for the related [2]catenane $\mathbf{17}^{4+}$.[15f,26] The nature of this rearrangement can be elucidated by the following observations: (i) the second oxidation of the TTF unit occurs at a potential value similar to that of the crown ether **5**, indicating that after the first oxidation the $TTF^{+\bullet}$ is no longer involved in strong CT interactions; (ii) the $TTF^{+/2+}$ wave is reversible, which shows that the system does not undergo any further rearrangement after one-electron oxidation; and (iii) the strongly positive potential value for the oxidation of the DNP unit indicates that, when this process occurs, the DNP moiety is encircled by the electron accepting cyclophane. These features show that, after the $TTF^{0/+}$ oxidation, the crown ether component circumrotates with respect to the electron accepting cyclophane, delivering the DNP unit into its cavity.

(34) Ashton, P. R.; Balzani, V.; Becher, J.; Credi, A.; Fyfe, M. C. T.; Mattersteig, G.; Menzer, S.; Nielsen, M. B.; Raymo, F. M.; Stoddart, J. F.; Venturi, M.; Williams, D. J. *J. Am. Chem. Soc.* **1999**, *121*, 3951–3957.

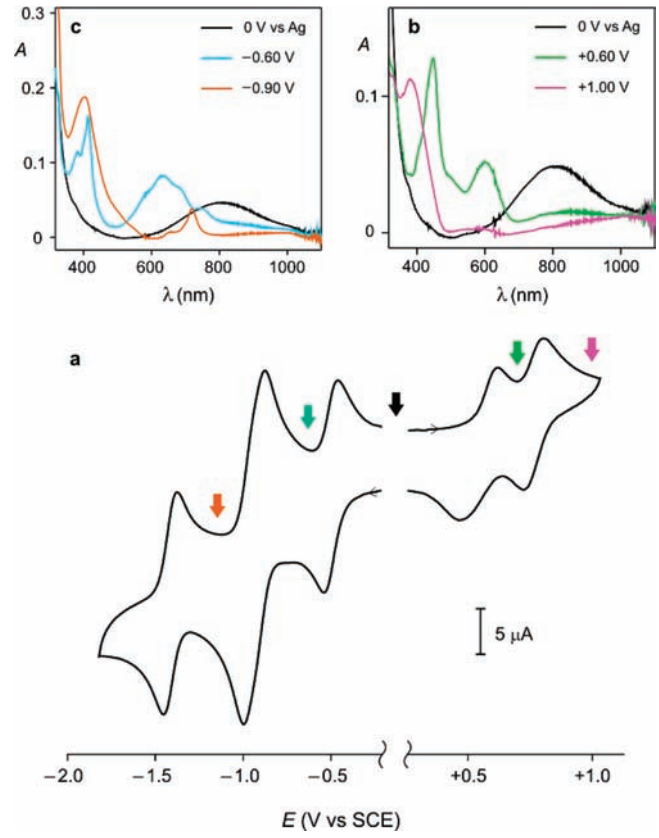


***Figure 9.*** Voltammetric and spectroelectrochemical response of catenane $\mathbf{8}^{2+}$ in $CH_3CN$ at room temperature. (a) Cyclic voltammetric curve ($4.9 \times 10^{-4}$ M, $TEAPF_6$ $7.3 \times 10^{-2}$ M, 200 mV/s, glassy carbon working electrode). (b) Absorption spectra observed before (black line) and after exhaustive oxidation at +0.60 V (green) and +1.00 V (pink) versus an Ag pseudoreference electrode. (c) Absorption spectra observed before (black line) and after exhaustive reduction at −0.60 V (blue) and −0.90 V (orange) versus an Ag pseudoreference electrode. Conditions for (b) and (c): $7.5 \times 10^{-4}$ M, $TEAPF_6$ $9.1 \times 10^{-2}$ M, platinum grid working electrode, optical path length 180 $\mu$m. The colored arrows in (a) mark the potential values at which the curves in (b) and (c) were recorded in the spectroelectrochemical experiments.

On the reduction side, the CV of $\mathbf{6}^{2+}$ reveals four reversible monoelectronic processes (Figure 8). The first one occurs at −0.42 V and can be assigned to the $BPY^{2+/+}$ reduction,[24] as confirmed by spectroelectrochemistry. The comparison with $\mathbf{15}^{4+}$ indicates[15c] that such a potential value is consistent with the reduction of a $BPY^{2+}$ unit engaged in CT interactions inside the cavity of **3**, in agreement with the dominant *co*-conformation of this [2]catenane. The second reduction takes place at −0.85 V and corresponds to the $BPY^{+/0}$ process according to spectroelectrochemical experiments. Although a unequivocal conclusion can hardly be drawn from our data, it is likely that the monoreduced $BPY^+$ unit remains inside the cavity of the crown ether, as is consistently observed in all other [2]catenanes (see sections below). The third (−0.98 V) and fourth (−1.53 V) processes are straightforwardly attributed to the $PMI^{0/-}$ and $PMI^{-/2-}$ reductions, respectively. The $PMI^{0/-}$ process in $\mathbf{6}^{2+}$ is negatively shifted by 160 mV with respect to **12**. In the related symmetric [2]catenane **18** that contains DNP moieties as the electron donors, the alongside PMI unit becomes harder to monoreduce by 120 mV with respect to a model species in $CH_2Cl_2$.[16b] Considering that HQ is a weaker electron donor than DNP, the rather large potential shift observed for the $PMI^{0/-}$ process in $\mathbf{6}^{2+}$ is not compatible with a PMI unit occupying an alongside position at the moment of its reduction. Hence, it is proposed that the process observed at −0.98 V is the reduction of the inside PMI unit. The translocation probably occurs upon reduction of the $BPY^+$ unit to its neutral form while the PMI unit becomes a better acceptor.

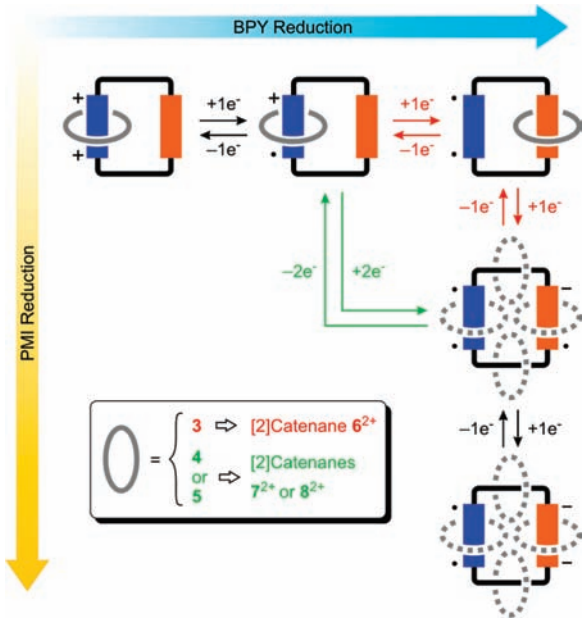


***Figure 10.*** *Co*-conformation changes associated with the four reduction processes for [2]catenanes $\mathbf{6}^{2+}$−$\mathbf{8}^{2+}$. Horizontal and vertical processes represent the BPY-centered and PMI-centered reductions, respectively. In the upper right part of the scheme, red arrows refer to the behavior of $\mathbf{6}^{2+}$, while green arrows describe the behavior of $\mathbf{7}^{2+}$ and $\mathbf{8}^{2+}$. The dotted gray ellipses indicate that the interactions are turned off and there is little information about the macrocycle location.

Our data are not sufficient to examine the positioning of the $PMI^{-}$ unit relatively to the crown ether ring. It is reasonable to consider, however, that the reduction of the PMI unit renders itself sufficiently electron-rich such that the stabilizing CT interactions are essentially turned off, and the crown ether component has no translational preference over either $BPY^{0}$ or $PMI^{-}$.

The cyclic voltammogram obtained upon reduction of $\mathbf{7}^{2+}$ consists of three reversible waves (Figure 8). Spectroelectrochemical experiments confirm that the first one (−0.54 V), which is monoelectronic, concerns the $BPY^{2+/+}$ process. A comparison with the behavior of [2]catenane $\mathbf{16}^{4+}$ indicates[15c] that the $BPY^{2+}$ unit occupies the inside position, as expected on the basis of the stable *co*-conformation of $\mathbf{7}^{2+}$. The second reduction wave (−0.95 V) involves the exchange of two electrons, which can be unambiguously assigned by spectroelectrochemistry to the overlapping $BPY^{+/0}$ and $PMI^{0/-1}$ processes.[35] A comparison with the behavior of [2]catenanes $\mathbf{16}^{4+}$ and **18** indicates that the $BPY^{+}$ and PMI units are inside and alongside, respectively. The third process (−1.50 V) is monoelectronic and corresponds to the $PMI^{-/2-}$ reduction.

The behavior of $\mathbf{8}^{2+}$ upon reduction (Figures 8 and 9) is qualitatively similar to that of $\mathbf{7}^{2+}$. Three reversible processes are observed. The first one (−0.50 V) is attributed to the first reduction of the inside $BPY^{2+}$ unit as evidenced by spectroelectrochemical measurements (Figure 9c) and by comparison with the potential values found for $\mathbf{17}^{4+}$.[15c] The second process (−0.92 V) is bielectronic and, for the same reasons discussed for $\mathbf{7}^{2+}$, is ascribed to the simultaneous reduction of the inside $BPY^{+}$ and alongside PMI units (Figure 9c). The third process (−1.41 V) is monoelectronic and is assigned to the $PMI^{-/2-}$ reduction. Overall, [2]catenane $\mathbf{8}^{2+}$ can be switched reversibly among as many as six states by both oxidation and reduction processes, but only the former ones can cause site-specific *co*-conformational changes.

The *co*-conformation changes coupled with the four-electron reduction processes for the PMI-containing [2]catenanes are summarized in Figure 10. In all cases, the electron rich crown ether remains encircling the $BPY^{+}$ radical cation after the first reduction, in keeping with the fact that $BPY^{+}$ is a better electron acceptor than the PMI unit. In the case of HQ-containing $\mathbf{6}^{2+}$, a site-specific *co*-conformational change accompanies the $BPY^{+/0}$ reduction process, leading to the translocation of the crown ether component onto the PMI unit. The successive $PMI^{0/-}$ reduction process increases the electron density such that donor−acceptor interactions become ineffective, possibly resulting in non site-specific shuffling of the crown ether component. In the case of [2]catenanes $\mathbf{7}^{2+}$ and $\mathbf{8}^{2+}$, the presence of more electron rich donors in the crown ether components further shifts the reduction potential of the $BPY^{+}$ radical cation such that it overlaps with the first reduction potential of the PMI unit. After this two-electron reduction, it is likely that the CT interactions are turned off, resulting in non site-specific *co*-conformational changes. It is notable that the site-specific *co*-conformational change associated with translocation of the crown ether component can be resolved in [2]catenane $\mathbf{6}^{2+}$, while in the case of $\mathbf{7}^{2+}$ and $\mathbf{8}^{2+}$ the coincidence of the $BPY^{+/0}$ and $PMI^{0/-}$ redox processes prevents an unambiguous *co*-conformational assignment.

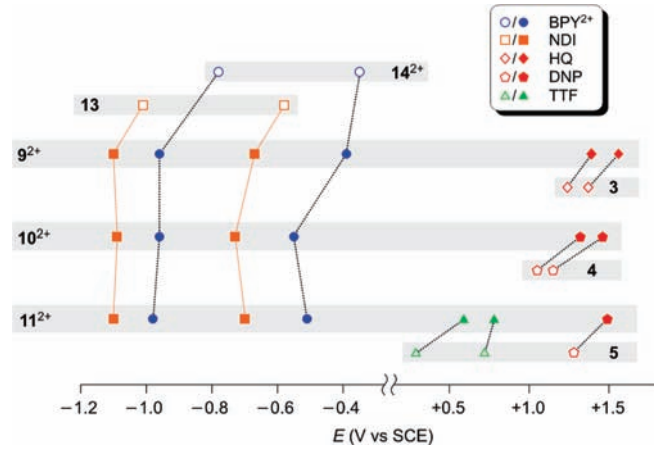


***Figure 11.*** Correlation diagram of the redox potentials of the [2]catenanes containing the NDI acceptor (filled symbols), and of their molecular components and model compounds (empty symbols).

**[2]Catenanes Containing the NDI Unit.** [2]Catenanes $\mathbf{9}^{2+}$ and $\mathbf{10}^{2+}$ (Figure 11) show two irreversible oxidative processes, assigned to the oxidation of the two HQ or DNP units of the crown ether component involved in CT interactions with the electron accepting cyclophane. The behavior of [2]catenane $\mathbf{11}^{2+}$ upon oxidation (Figure 11) is very similar to that exhibited by $\mathbf{8}^{2+}$, which indicates that the $TTF^{0/+}$ oxidation causes the circumrotation of the crown ether component with respect to the cyclophane to position the DNP moiety into its cavity.

The reduction pattern for all three [2]catenanes comprises four reversible monoelectronic processes (Figure 11). With the help of spectroelectrochemistry and by comparison with the model compounds, such processes can be assigned to $BPY^{2+/+}$, $NDI^{0/-}$, $BPY^{+/0}$, and $NDI^{-/2-}$, respectively, in the order of increasing reduction potential. The proposed *co*-conformational changes coupled with the four one-electron reduction processes for these [2]catenanes are also very similar (Figure 12). Taking $\mathbf{9}^{2+}$ as the example, the electron-rich component **3** remains around the $BPY^{+}$ radical cation after the first reduction. The second reduction (−0.67 V), which is negatively shifted by 90 mV with respect to model **13**, is indicated by spectroelectrochemical experiment to be the $NDI^{0/-}$ process.[35] The experiments on the model [2]catenane **19** show that in $CH_2Cl_2$ the alongside and inside NDI units become harder to reduce by 100 and 380 mV, respectively, with respect to the NDI model compound.[16b] Hence, even considering that the HQ unit is a weaker donor than DNP, the potential value found for the $NDI^{0/-}$ process in $\mathbf{9}^{2+}$ is more consistent with the reduction of the NDI moiety in the alongside position. Accordingly, the crown ether component still encircles the monoreduced $BPY^{+}$ unit. This interpretation is

(35) Gosztola, D.; Niemczyk, M. P.; Svec, W.; Lukas, A. S.; Wasielewski, M. R. *J. Phys. Chem. A* **2000**, *104*, 6545–6551.

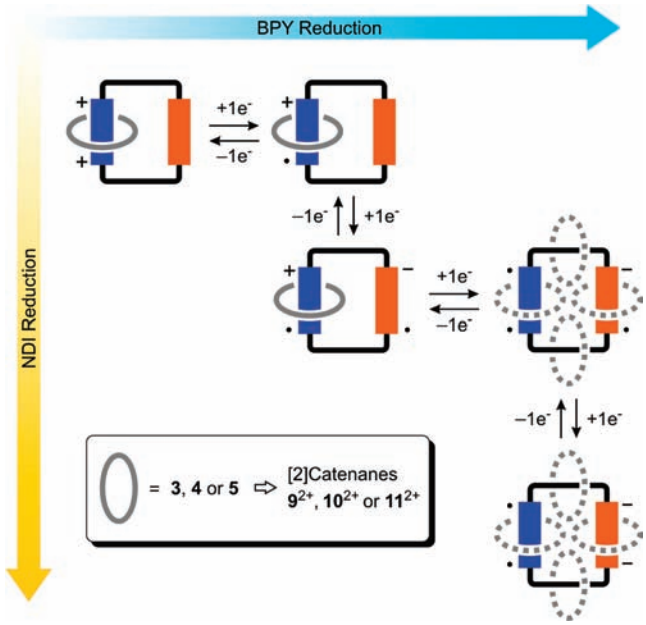


***Figure 12.*** *Co*-conformational changes associated with the four reduction processes for [2]catenanes $\mathbf{9}^{2+}$−$\mathbf{11}^{2+}$. Horizontal and vertical processes represent the BPY-centered and NDI-centered reductions, respectively. The dotted gray ellipses indicate that the interactions are turned off and there is little information about the macrocycle location.

further supported by the remarkably negative potential value (−0.96 V) found for the third reduction wave, that can be assigned to the $BPY^{+/0}$ process. The fourth process (−1.10 V) is the $NDI^{-/2-}$ reduction. As noted previously for the PMI-based catenanes, our results do not enable to discuss the positioning of the $NDI^-$ unit relatively to the crown ether ring. However, one can reasonably assume that upon reduction the NDI unit loses its electron-accepting properties and is no longer involved in CT interactions with the electron donor ring, which in turn should not preferentially encircle either $BPY^0$ or $NDI^-$. A similar analysis applies to the reduction of [2]catenanes $\mathbf{10}^{2+}$ and $\mathbf{11}^{2+}$. It is noteworthy that [2]catenane $\mathbf{11}^{2+}$ can be switched reversibly among as many as seven states both by reduction (Figure 12) and oxidation processes, but only the latter ones can cause site-specific macrocycle circumrotation.

To gain more insight into the nature of the intercomponent interactions in these systems, a comparison between the spectroscopic and the electrochemical data can be attempted. Specifically, if the dominant interaction between the molecular units is the charge-transfer one, it may be expected to observe a correlation between the electronic coupling elements estimated from the CT absorption bands ($H_{DA}$, Table 2) and the shifts in the potentials for the first reduction and oxidation processes experienced by the molecular components when they are mutually interlocked ($|\Delta E_{red}| + |\Delta E_{ox}|$, Table 3). It should be noticed, however, that the solvation effects associated with the CT optical transition are different from those associated with the individual (reduction or oxidation) electrochemical processes.

First of all, the values of $H_{DA}$ and potential shift for the interaction involving a given donor−acceptor pair do not depend on the specific [2]catenane structure (for example, $\mathbf{8}^{2+}$ or $\mathbf{11}^{2+}$ in the case of the TTF-$BPY^{2+}$ interaction). This result supports the idea that these species are characterized by a prevailing CT interaction, which takes place between the best donor and acceptor units. The most interesting observation, however, is that the shift in the redox potentials exhibited by the [2]catenanes containing crown ether **5** is smaller than that shown by the [2]catenanes of macrocycle **4**, in spite of the larger electronic coupling of the $BPY^{2+}$ unit with TTF compared with DNP. Presumably, other factors besides the CT interaction (e.g., steric and conformational effects) affect the redox potentials of the electroactive units in the [2]catenanes.

## Conclusion

We have synthesized a series of desymmetrized donor−acceptor [2]catenanes where different donor and acceptor units are assembled within a confined catenated geometry. Remarkable translational selectivity is maintained in all cases, including two fully desymmetrized [2]catenanes where both donors and acceptors are different, as revealed by $^1$H NMR spectroscopy and X-ray single crystal structures. It is consistent that in all desymmetrized [2]catenanes the *co*-conformation is dominated by the strongest donor and acceptor pairs, whose charge-transfer interactions also determine the visible absorption properties The *co*-conformations can be switched by chemically or electrochemically altering the redox state of these donors and acceptors. As shown by electrochemical studies, the uptake of electrons frustrates the $\pi$-accepting properties of the bipyridinium and bis-imide moieties. The inside/alongside topological preference, dominated by the intercomponent CT interactions, can be modulated reversibly upon reduction of the electron acceptors, or oxidation of the electron donors in the cases of fully desymmetrized **8**•$2PF_6$ and **11**•$2PF_6$. Such a feature makes these catenanes appealing structures for the construction of molecular machines and, in a perspective, rotary motors. It should also be noted that these interlocked molecules can be reversibly switched among several states, characterized by distinct electronic and optical properties, by electrochemical stimulation in a relatively narrow and easily accessible potential window. Such a possibility could open interesting routes for the development of molecular electronic devices that go beyond binary logic.

**Acknowledgment.** Dedicated to Professor Jean-Pierre Sauvage, pioneer of molecular catenation, for his 65th birthday. D. Cao, L. Klivansky, G. Koshkakaryan, and Y. Liu and the materials synthesis were supported by the Office of Science, Office of Basic Energy Sciences, of the U.S. Department of Energy under contract No. DE-AC02-05 CH11231, M. Amelia, M. Semeraro, S. Silvi, M. Venturi, and A. Credi and the detailed characterization were supported by Fondazione Cassa di Risparmio in Bologna, Italy.

**Supporting Information Available:** Experimental details and characterization data of all new compounds. Crystallographic information files (CIF) of **8**•$2PF_6$, **9**•$2PF_6$ and **11**•$2PF_6$. Variable temperature $^1$H NMR spectra of the [2]catenanes. $^1$H NMR spectra showing the chemical switching process of **8**•$2PF_6$. This material is available free of charge via the Internet at http://pubs.acs.org.

JA909041G